University of Manitoba

Honours Thesis

Study on Coherent Coupling Between Magnons and Microwave Photons in an Active Planar Resonator

Author:
Yutong Zhao

Supervisor:
Can-Ming Hu

A thesis submitted to the Department of Physics and Astronomy in partial fulfillment of the requirements for the honours physics thesis

April 9, 2018

Abstract

We studied the spin-photon interaction in an active cavity with a voltage controlled feedback loop at room temperature. In order to study this phenomenon, an active cavity with A-P design was fabricated with a tunable range of Q factor from 10^2 to 10^5. In this work, we experimentally demonstrated that the coupling strength, in this specific configuration, can be controlled by the number of feedback photons and polaritons through tuning the bias voltage and distance, respectively. Feedback loop is commonly used in engineering and scientific research, the emergence of active cavity would extend the field of cavity magnon polariton. This leads to a better understanding of the coupling between magnon and feedback cavities and provides a new perspective for fundamental coupling in spintronics.

Contents

1 Introduction

Light-mater interaction is a long standing topic in physics. Interaction between light and materials give rise of lots of common phenomena such as diffraction, reflection, deflection, et cetera... These phenomena depend on permeability and permittivity of material. The interaction of these effects are weak which means that electronic states of the medium remain same during the process [1]. When the interaction is strong enough to alternate the electronic states of the medium, a type of quasi-particle known as "polariton" is generated whose behavior is the superposition properties of photons and matter. Polariton was first theoretically predicted by Tolpygo [2] and Huang [3] independently who had studied the interaction between the electromagnetic field and phonon in crystals. This lead to the emergence of phonon-polariton which involves crystal motion and light. After the discovery of polariton, this area of research has evolved greatly over years during which different types of polaritons were theoretically and experimentally studied [4]. For example, exciton-polariton and plasmon-polariton. The combination of spintronics and polariton gives rise to new fields of light-matter interaction such as magnon polariton (magnon with microwave photon) which is based on magnetic material interacting with light [5].

1.1 Ferromagnetic Resonance and Magnon

Ferromagnetic resonance is one of the most exciting discoveries in the mid-20th century of solid state physics. In 1935, Lev Landau and Evgeny Lifshitz first predicted microwave absorption due to the procession motion of magnetic moment in a static magnetic field for ferromagnetic materials [6]. In late 1940s, experiments were performed and verified by J. H. E. Griffiths who observed energy loss in high frequency current by using a thin ferromagnetic metal [7]. Russian scientist E. K. Zavoiskij discovered the same phenomenon through using paramagnetic salts in the same year independently [8, 9]. Later Kittel discussed the theory on dispersion of these Ferromagnetic Resonance(FMR) in different structures which now is known as the "Kittel formula" [10].

The mechanism of Ferromagnetic Resonance(FMR) is broadly similar to electron paramagnetic resonance(EPR) and nuclear magnetic resonance(NMR). The difference is that FMR probes magnetic moment resulting from unpaired electrons and NMR probes the magnetic moment of nuclei. In modern physics research, FMR as a spectroscopic technique that commonly studied together with microwave cavities has become a tool of probing spin wave in spintronics and spin dynamics.

Spin wave is formed and propagated in a magnetic material if a perturbation is acting on local magnetic ordering [11]. Bloch first predicted spin wave [12] and later scientists realized it was the result from collective excitations of the electron spins in ferromagnetic materials. Today, spin wave is considered as a promising candidate for next generation information transporting and processing [13]. Quantised spin waves, known as magnons, are a type of quasiparticles like phonon. A fixed amount of energy, lattice momentum and integer spin number are carried by magnons resulting they obey Bose-Einstein statistics.

1.2 Microwave cavity and Cavity Photon

Microwave cavity, also known as resonator, is a design of certain structure that is able to confine the electromagnetic fields in the microwave region of spectrum. Standing waves are formed in the resonator by photons bouncing back and forth between the wall of the cavity this yield resonant peaks or absorption dips in spectrum at certain frequencies. While the cavity is in resonance, electric and magnetic energy is stored within the cavity and dissipated gradually due to variously damping mechanisms such as Ohm loss and dielectric loss [14]. Furthermore, if the cavity has an open boundary such as in planar structures, the energy would also radiate to environment [15]. The quality factor Q, is a dimensionless value describes how efficiently the cavity is able to store energy. The higher Q the cavity have, the sharper the resonant peak is on spectrum. An efficient cavity will have a long average photon lifetime which provides a great convenience for particles to interact with each other. Generally, high Q cavities are preferred in research.

Microwave cavities have different designs that vary from 2-D to 3-D. At room temperature, 3-D metallic cavity often have a Q of a few thousand therefore it has been commonly adopted as microwave cavities in research. Even though 3-D cavities give beautiful results it faces difficulties in application such as fabricating, integrating and manipulating [16]. Planar structure was used in this work to overcome this drawback. For 2-D microstrip resonator, the Q factor is usually on the order of several hundred due to its relatively high loss. Traditional passive planar cavities usually have a Q value limit around several hundred which brings difficulties for interaction. In principle, any structure can have resonant modes. However, the microstrip resonators are usually designed in rectangular, split-ring or circular. Different cavity geometries result in different boundary conditions, which would result in different solutions to the Maxwell equations and correspond to distinct resonant frequencies, Q factors and

field spatial distributions.

The active cavity was firstly designed for acquiring high Q cavities by integrating an feedback loop circuit on passive resonators [17]. Soon after it has found great applications in sensitive measurements such as liquid sensing [18] and organic-vapor sensing [19]. Apart from the high sensitive measurement, this high Q resonator provided a novel perspective for fundamental research in solid state physics especially in spin dynamics. With the assistance of external voltage sources and an amplifying circuit, the resonance signal with certain frequency is amplified and Q factor is increased by 3 orders of magnitude (from 10^2 to 10^5) [20]. Therefore, active resonators provide a new approach to study the light-matter coupling.

1.3 Emergence of Cavity Magnon Polaritons

The discovery of cavity-magnon-polariton(CMP) whose focus is on spin-photon interaction provides a newly emerging sub-field [15,20–27] in light-matter interaction. The theoretical prediction of the strong coupling between cavity photons and magnons was made in 2010 [28] and was first experimentally demonstrated in 2013 at low temperature [29]. Soon after, the experiment in room temperature was achieved by coupling a YIG sphere and a 3D microwave cavity by Zhang et al [26]. In order to illustrate the CMP system, a schematic diagram of CMP was given in Fig.1. The coupling strength g indicates the speed of the energy exchange between photon and magnon with dimension of s^{-1}. γ_c and γ_m are the dispassion rate of the cavity photon and magnon that indicate energy is lost rate. By tuning coupling and damping of the system, CMP can reach various coupling regimes (strong coupling, weak coupling, magnetically induced transparency and Purcell effect) [26] of which each has distinct properties. CMP is given by coherent coupling whose definition is given by the cooperativity greater than unity ($C = \dfrac{g^2}{\gamma_m \gamma_c} > 1$) [30] which indicate energy exchange can complete at least one cycle before the energy is damped away.

Research in CMP has lead to development of various potential practical applications such as quantum transducer that is able to coherently connect various quantum systems [31], device that is able to precisely control and readout the information stored in qubit states [32] and so on. Following the development of the CMP, our focus is on coherent coupling between microwave photons and magnons. In previous CMP research [26,32], passive resonator was widely used to generate cavity photons that couple with magnons. Combining the active cavity with magnons results expansion of CMP. For instance, Yao et al reported a completely new phenomenon called

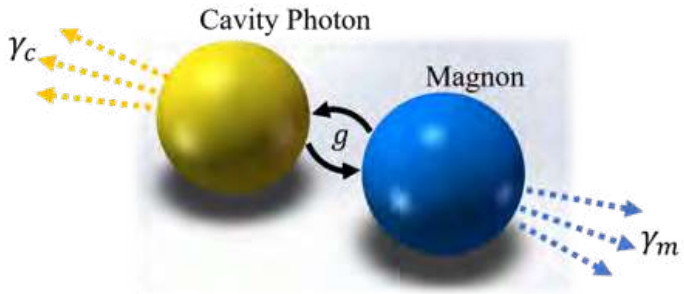

Figure 1: Schematic diagram of Cavity Magnon Polaritons: cavity photons interact with magnons. g is the coupling strength showing how strong is the interaction, γ_c and γ_m is the damping rate of cavity photon and magnon which represent how fast the energy lost from these two particles.

magnon quintuplet and observed breaking of harmonic-oscillator restriction by using an active cavity and ferromagnetic sphere [20]. Following their work, it is important to study the feedback effect in polariton dynamics with a feedback-coupled cavity and determine what kind of variables effect coupling. In this work, a similar active resonator was designed and fabricated. The target is to study the influence of the active cavity with a feedback loop on coherent coupling in a planar structure by using a Yttrium iron garnet(YIG) sphere.

2 Theory

2.1 Cavity mode

2.1.1 RLC circuit model

Microwave resonator in this research is made by microstrip which has a top layer of metal to convey microwave and form cavities, a layer of dielectric substrate in middle and a ground bottom layer. An intuitive understanding of the microwave cavity is using its equivalent RLC circuit to model the microwave cavity photons and magnons (shown in Fig.2).

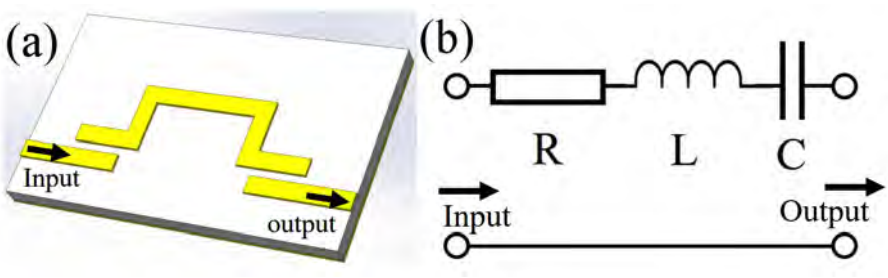

Figure 2: (a) A typical open-end microstrip resonator with long feed line fabricated from print circuit board (PCB) technology. Signal is sending in from LHS and extracting out from RHS. (b) The equivalent RLC circuit of open-end microwave cavity shown in (a).

To characterize RLC circuit, it is necessary to know the input/output of the system. We firstly write down the frequency dependent impedances of the resistance, inductance and capacitor:

$$Z_R = R \qquad Z_L = iL\omega \qquad Z_c = \frac{1}{iC\omega} \tag{1}$$

It is easy to obtain the net impendence as:

$$Z_s = R + i\omega L + \frac{1}{i\omega C} \tag{2}$$

The impendence of the RLC circuit shown in Fig.2 can be reorganized as

$$Z_s = \frac{(\omega_0 - \omega) + i\Delta\omega/2}{ig/2} \tag{3}$$

Where $g = 1/L$ is the coupling strength between resonator and feed lines, $\omega_0 = 1/\sqrt{LC}$ gives the resonance peak position and $\Delta\omega = R/L$ is the linewidth. Also the approximation $\omega + \omega_0 \approx 2\omega$ has been applied in the derivation.

In order to compare theoretical value and measurement data, we introduce the transmission(ABCD) matrix and scattering (S parameters) matrix (see Fig.3 Two-port network) whose definitions are given by:

$$\begin{pmatrix} V_1 \\ I_1 \end{pmatrix} = \begin{pmatrix} A & B \\ C & D \end{pmatrix} \begin{pmatrix} V_2 \\ I_2 \end{pmatrix} \qquad \text{and} \qquad \begin{pmatrix} b_1 \\ b_2 \end{pmatrix} = \begin{pmatrix} S_{11} & S_{12} \\ S_{21} & S_{22} \end{pmatrix} \begin{pmatrix} a_1 \\ a_2 \end{pmatrix} \tag{4}$$

where V_1, I_1 are the input voltage and current applied at Port 1; whereas, V_2, I_2 are the output voltage and current at Port 2. The advantage of using the transmission matrix is that for a cascade connection of two port networks, the overall transmission

matrix can be found by simply multiplying the transmission matrix for each individual network as following:

$$\begin{bmatrix} V_{\text{input}} \\ I_{\text{input}} \end{bmatrix} = [M_1][M_2]\cdots[M_n] \begin{bmatrix} V_{\text{output}} \\ I_{\text{output}} \end{bmatrix} \tag{5}$$

The transmission matrix of RLC resonator like Fig.2(b) is given by [33]:

$$[M_{ABCD}] == \begin{pmatrix} 1 & Z_s \\ 0 & 1 \end{pmatrix} \tag{6}$$

However the drawback of using the ABCD matrix is that it is difficult to measure microwave current and voltage. Experimentally, we measure the scattering parameters (S parameters) directly using a vector network analyser(VNA). Relation of between transmission matrix and scattering matrix(shown in Fig.3(b)) is given by [33]:

$$\begin{aligned} [S] &= \begin{bmatrix} S_{11} & S_{12} \\ S_{21} & S_{22} \end{bmatrix} \\ &= \begin{bmatrix} \dfrac{A + B/Z_0 - CZ_0 - D}{A + B/Z_0 + CZ_0 + D} & \dfrac{2(AD - BC)}{A + B/Z_0 + CZ_0 + D} \\ \dfrac{2}{A + B/Z_0 + CZ_0 + D} & \dfrac{-A + B/Z_0 - CZ_0 + D}{A + B/Z_0 + CZ_0 + D} \end{bmatrix} \end{aligned} \tag{7}$$

The S-parameters S_{ij} of an active or passive microwave network are the ratios of the voltage waves emitted from port j, to the voltage waves received from port i.

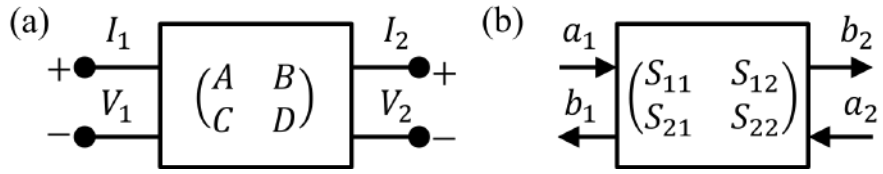

Figure 3: Two port network: (a) Transmission (ABCD) matrix, V_1,V_2 (I_1,I_2) are the voltage cross(current through) port 1(left) and port 2(right) (b) Scattering matrix that describes the amplitude and phase difference between initial and final states using complex values for input a_1,a_2 and output b_1,b_2.

Z_0 is the impendence of the measurement instrument usually taken to be 50 Ω.

Substituting the ABCD of our system, we can acquire the S_{21} parameter(transmission):

$$|S_{21}| = \left| \frac{igZ_0}{(\omega_0 - \omega) + i(\Delta\omega + gZ_0)} \right| \tag{8}$$

2.1.2 Classical Oscillator

Another method to characterize the photon cavity is using a classical driven damped oscillator.

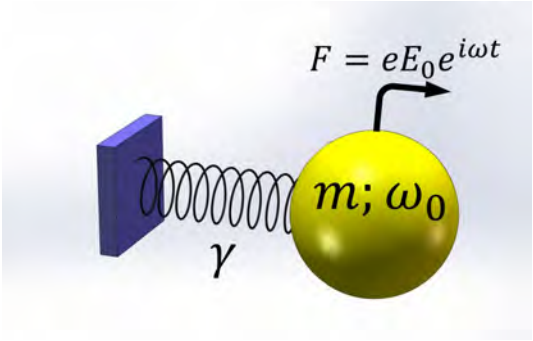

Figure 4: Damped Oscillator Model describe a dipole in electromagnetic field, a spring connect with a mass point m that driven by a periodic force F which gives an intrinsic resonant frequency Ω_0, e is the charge carried by the dipole and E_0 is the electric field strength. Damping γ slows the motion proportion to the velocity $\dot{x}$.

Consider a linear dipole oscillates in an electromagnetic field:

$$E(t) = E_0 e^{i\omega t} \tag{9}$$

Such system can be described by driven harmonic oscillation, the equation of motion is given by:

$$\ddot{x} + \gamma\omega_0\dot{x} + \omega_0^2 x = fe^{i\omega t} \tag{10}$$

where ω_0 is the intrinsic oscillation frequency of the electric dipole, and $f = eE_0/m$ is the maximum force acting on the oscillator. we assume that position of oscillator $x(t)$ can be described by a complex amplitude $X(t)$ and the periodic force:

$$x(t) = X(t) \cdot e^{i\omega t} \tag{11}$$

substituting into equation of motion we can get:

$$(\ddot{X} + 2i\omega\dot{X} - \omega^2 X) + \gamma\omega_0(\dot{X} - i\omega X) + \omega^2 X = f \tag{12}$$

In most of the cases, $\ddot{X}$ and $\gamma\dot{X}$ are very small quality, so we have:

$$2i\omega\dot{X} - \omega_0^2 X + \omega^2 X - i\gamma\omega\omega_0 X = f \tag{13}$$

In order to obtain steady-state solution, we set the first derivative of the amplitude to zero ($\dot{X} = 0$).

$$X = \frac{f}{\omega^2 - \omega_0^2 + i\gamma\omega\omega_0} \tag{14}$$

When the system is near resonance, we have $|\omega - \omega_0| << \omega + \omega_0$. Therefore, we can make approximation:

$$\omega_0^2 - \omega^2 \approx 2\omega(\omega_0 - \omega) \tag{15}$$

So we have the approximated amplitude as :

$$X = \frac{f}{\omega_0 - \omega + i\gamma\omega_0/2} \tag{16}$$

which gives a lorentz line shape resonance. If we have a weak spring that can extract a very small portion of energy and that has no influence on over original motion, then we can acquire the S parameter of the system which is proportional to the amplitude X. The solution of x may not be exactly in phase of the driving force. Thus, the solution will have a form with additional phase shift ϕ can be write as $X \cdot e^{i(\omega t+\phi)}$. The expression of the phase shift from Eq.14 is frequency dependent:

$$tan(\phi(\omega)) = \frac{\omega\gamma}{\omega_0^2 - \omega^2} \tag{17}$$

From this formula a difference of $\pm(\pi/2)$ off resonance and 0 in resonance can be expected, the result is shown in Fig.5(c,d).

2.1.3 Cavity Photon Hamiltonian

The microwave cavity can be described by a quantum harmonic oscillator model if we know the particle mass as m and the force constant as k. The Hamiltonian can be write as the sum of kinetic energy and potential energy:

$$\hat{H} = \frac{\hat{p}^2}{2m} + \frac{1}{2}k\hat{x}^2 = \frac{\hat{p}^2}{2m} + \frac{1}{2}m\omega^2\hat{x}^2 \tag{18}$$

Where $\hat{x}$ is the position operator given by $\hat{x} = x$ and $\hat{p}$ is the momentum operator given by $\hat{p} = -i\hbar\frac{\partial}{\partial x}$. The intrinsic angular frequency ω is given by $\sqrt{k/m}$. The eigenvalue E of this system can be acquired by solving the time-independent

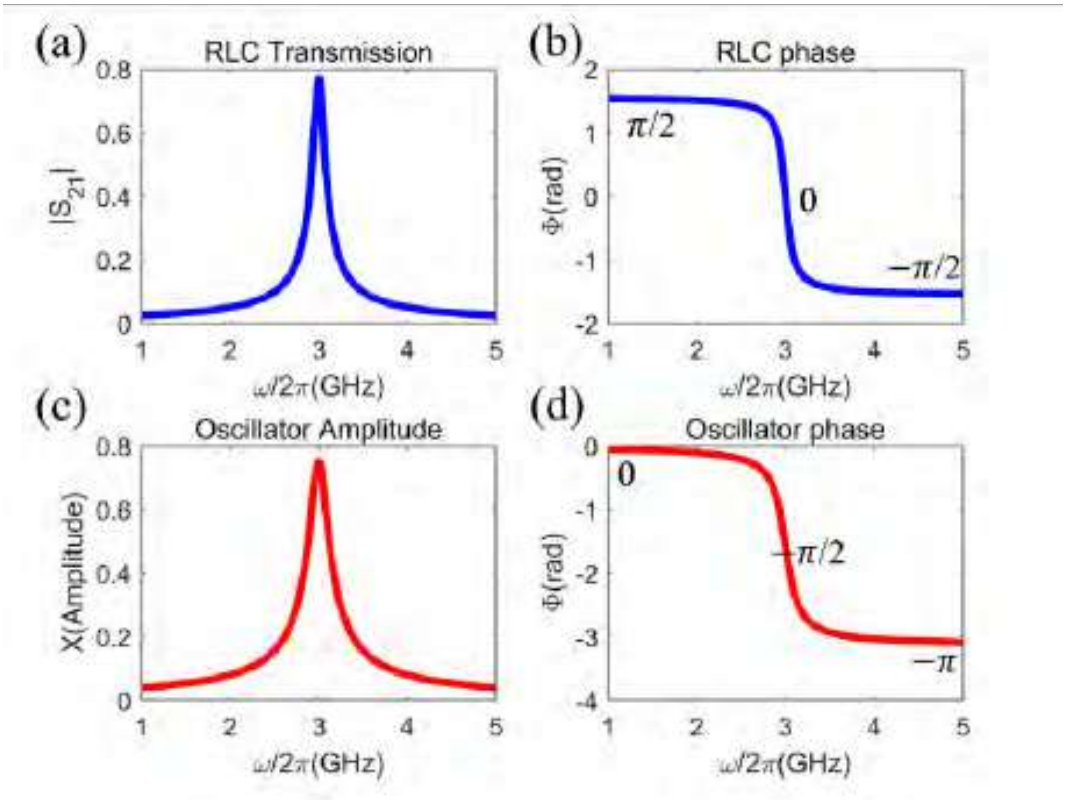

Figure 5: (a)S_{21} parameter of the RLC model, numerical calculation for R = 30Ω, L = $1.0\mu H$ and C = $0.11pF$. (b)S_{21} Phase difference of RLC model, the phase shift in resonance is 0 and off resonance is $\pm\pi/2$(c)(d) Amplitude and Phase difference for damped oscillator model, numerical calculation for ω_0 = 3GHz, γ = 0.5GHz and Amplitude = 0.8. From the four graphs in figure, we can know that RLC circuit and damped oscillator yield a similar result.

Schrodinger equation:

$$\hat{H}\,|\psi\rangle = E\,|\psi\rangle \tag{19}$$

Using ladder operator method, we define the creation operator $\hat{a}^\dagger$ and annihilation operator $\hat{a}$ which is given by:

$$\begin{aligned} \hat{a} &= \sqrt{\frac{m\omega}{2\hbar}}(\hat{x} + \frac{i\hat{p}}{m\omega}) \\ \hat{a}^\dagger &= \sqrt{\frac{m\omega}{2\hbar}}(\hat{x} - \frac{i\hat{p}}{m\omega}) \end{aligned} \tag{20}$$

The operators act on a quantum state $|n\rangle$ and yields:

$$\begin{aligned} \hat{a}^\dagger |n\rangle &= \sqrt{n+1}\,|n+1\rangle \\ \hat{a}\,|n\rangle &= \sqrt{n}\,|n-1\rangle \end{aligned} \tag{21}$$

The Hamiltonian using the ladder operators can be rewrite as:

$$\hat{H} = \hbar\omega(\hat{a}^\dagger\hat{a} + \frac{1}{2}) \tag{22}$$

Consider the energy stored in the oscillator as the Hamiltonian of cavity photons:

$$\hat{H}_{\text{magnon}} = \delta\hat{H} = \hbar\omega\hat{a}^\dagger\hat{a} \tag{23}$$

2.2 Magnon

2.2.1 Ferromagnetic Resonance

A material is called ferromagnetic if its spins tend to align a certain direction spontaneously or under external field below the Curie temperature T_c. In order to excite (FMR), the magnetization of the material is aligned with an externally applied direct current magnetic field, and a microwave frequency field is then used to drive magnetization precession. This can be explained by the spin polarization, arising due to the exchange interaction within the atomic lattice making it energetically favourable for the spins of neighboring atoms to align, which will result in a local non-zero magnetization.

A mathematical description of FMR usually begin with damping free Landau-Lifshitz equation:

$$\frac{d\vec{M}}{dt} = -\gamma(\vec{M} \times \vec{H}_{\text{eff}}) \tag{24}$$

Where H_{eff} is the effective internal field that felt by magnetization $\vec{M}$ and γ is the electron gyromagnetic ratio. H_{eff} contains two parts, one from the static internal field due to the electromagnet and the other from the periodic oscillating microwave magnetic field:

$$\vec{H}_{\text{eff}} = \vec{H}_{\text{static}} + \vec{h}_0 e^{i\omega t} \tag{25}$$

Based on phenological facts we introduce a damping term that produces a torque forces the magnetization move inward and reduce the cone angle of the precession.

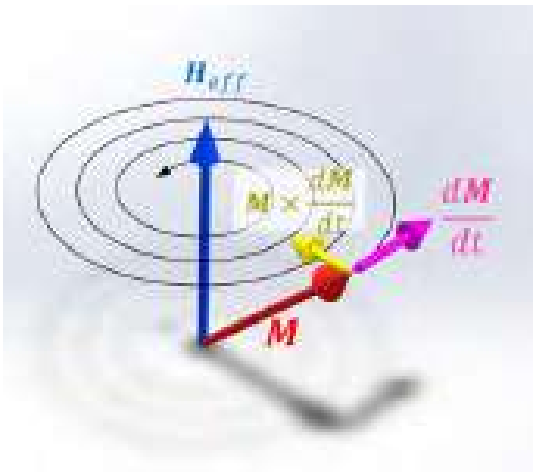

Figure 6: Schematic diagram for ferromagnetic resonance characterized by LLG equation. The magnetization M (red arrow) precess alone the effective internal field H_{eff} (blue arrow). Where the damping is given by the $M \times \frac{dM}{dt}$(yellow arrow) and the velocity of the precession movement is $\frac{dM}{dt}$ (purple arrow). The $\vec{M}$ would eventually align towards the z direction follows the spiral curve if without the microwave field.

With damping the Landau-Lifshitz equation becomes:

$$\frac{d\vec{M}}{dt} = -\gamma(\vec{M} \times \vec{H}_{\text{eff}}) + \lambda(\frac{(\vec{H} \cdot \vec{M})\vec{M}}{M^2} - H_{\text{eff}}) \tag{26}$$

where λ is the Landau-Lifshitz damping parameter, and has the dimensions of frequency(s^{-1}). By using the BAC$-$CAB rule $\vec{A} \times (\vec{B} \times \vec{C}) = \vec{B}(\vec{C} \cdot \vec{A}) + \vec{C}(\vec{A} \cdot \vec{B})$, we have

$$\frac{d\vec{M}}{dt} = -\gamma(\vec{M} \times \vec{H}_{\text{eff}}) - \lambda(\frac{\vec{M} \times (\vec{M} \times \vec{H_{\text{eff}}})}{M^2}) \tag{27}$$

Whereα is the Gilbert damping parameter defined as:

$$\alpha = \frac{\lambda}{\gamma M} \tag{28}$$

So we have:

$$\frac{d\vec{M}}{dt} = -\gamma(\vec{M} \times \vec{H}_{\text{eff}} - \frac{\alpha\gamma}{M}(\vec{M} \times (\vec{M} \times \vec{H}_{\text{eff}}))) \tag{29}$$

we can then cross the

$$\gamma\vec{M} \times (\vec{M} \times \vec{H}_{\text{eff}}) = -\vec{M} \times \frac{d\vec{M}}{dt} + \alpha\gamma M(\vec{M} \times \vec{H}_{\text{eff}}) \tag{30}$$

We have acquired the Landau-Lifshitz-Gilbert (LLG) equation that commonly used

$$\frac{d\vec{M}}{dt} = -\gamma(\vec{M} \times \vec{H}_{\text{eff}})(1+\alpha^2) + \frac{\alpha}{M}(\vec{M} \times \frac{\vec{M}}{dt}) \tag{31}$$

The LLG equation is a non-linear partial differential equation, for the cases when the procession angle is small, it can be approximated by linear analytical solutions. However, when procession angle is large enough by increasing the power of microwave, non-linear effect would appear. The α^2 term is far smaller than one ($\alpha \ll 1$), therefore, this term is neglected in most cases. From the Eq.31 we can derive reaction of magnetization under a periodically changing magnetic field. The first term of the LLG equation characterizes the torque induced by the applied static magnetic field, the analog in a precessing top is the torque exerted by gravity. The second term produces an inward force that tend to reduce the rotation angle which results in the dispassion of this procession motion (see Fig.6). In experiment, if the torque induced by the magnetic field of the microwave cancels the damping term, we see a strong absorption in transmission spectrum.

Suppose the static external field towards Z direction has a value h_{ext} and microwave only acts on x-y plane, the effective internal magnetic field from Eq.25 and internal magnetization can be write as below:

$$\begin{aligned} \vec{H}_{\text{ext}} &= [h_x e^{i\omega t}, h_y e^{i\omega t}, h_0 + h_z e^{i\omega t}] \\ \vec{M} &= [m_x e^{i\omega t}, m_y e^{i\omega t}, m_0] \end{aligned} \tag{32}$$

Internal fields will not be the same as the externally applied fields $\vec{H}_{\text{ext}} = (h_{ex}, h_{ey}, h_{e0})$ but can be related to the external field through the demagnetization factors $\vec{n} = (n_x, n_y, n_z)$, which depend on the sample geometry and are taken to be uniform in a given direction. Therefore, the external field has a following relation with magnetization of sample:

$$\vec{H}_{\text{ext}} = \vec{h}_{\text{eff}} - \vec{n} \cdot \vec{M} \tag{33}$$

Consider the damping free case in Eq.24, the left hand side become:

$$-\gamma\vec{M}\times\vec{H}_{\text{eff}} = -\gamma \begin{pmatrix} \hat{x} & \hat{y} & \hat{z} \\ m_x e^{i\omega t} & m_y e^{i\omega t} & m_0 \\ h_x e^{i\omega t} & h_y e^{i\omega t} & h_0 + h_z e^{i\omega t} \end{pmatrix} = -\gamma e^{i\omega t} \begin{pmatrix} m_y h_0 - m_0 h_y + m_y h_z e^{i\omega t} \\ m_0 h_x - m_x h_0 - m_x h_z e^{i\omega t} \\ (m_x h_y - h_x m_y) e^{i\omega t} \end{pmatrix} \tag{34}$$

In this case, m_x,m_y and h_x, h_y are usually small quantity compare to m_0 and h_0,

therefore, any two of these product is approximately zero. and the right hand side is easy to obtain:

$$\frac{d\vec{M}}{dt} = i\omega e^{i\omega t}[m_x, m_y, 0] \tag{35}$$

Now we acquire two equations by using approximations:

$$\begin{aligned} -\gamma(h_{e0} + m_0(n_y - n_z))m_y + i\omega m_x = 0 \\ -\gamma(h_{e0} + m_0(n_z - n_y))m_x + i\omega m_y = 0 \end{aligned} \tag{36}$$

to rewrite in matrix form we have:

$$\begin{pmatrix} -i\omega & -\gamma(h_e 0 + m_0(n_y - n_z)) \\ -\gamma(h_{e0} + m_0(n_z - n_y)) & -i\omega \end{pmatrix} \begin{pmatrix} m_x \\ m_y \end{pmatrix} = \begin{pmatrix} 0 \\ 0 \end{pmatrix} \tag{37}$$

where the n_y and n_x are defined as h_y/m_x and h_x/m_x, respectively. Using the determinant of matrix we can derive the dispersion relation:

$$\omega^2 - \gamma^2(h_{e0} + m_0(n_y - n_z))(h_{e0} + m_0(n_x - n_z)) = 0 \tag{38}$$

For a spherical sample, the demagnetization factors are given as $n_x = n_y = n_z$ due to the symmetric property. Therefore, we have:

$$\omega = \gamma h_{e0} \tag{39}$$

We have proved the dispersion relation of a spherical sample is linear as with respect to the external magnetic field.

2.2.2 Collective Spin Hamiltonian

Suppose the ground state of the ensemble of identical two-level atoms are expanded by a set of 2^N orthogonal states such as $|g\rangle_1 |g\rangle_2 ... |g\rangle_N$, where N is the total number of atoms. The operator $\hat{S}$ for collective spin that represent the internal state of N atoms is:

$$\hat{S}_i = \frac{1}{2}\sum_{n=1}^{N} \sigma_{ni} \quad (i = x, y, z) \tag{40}$$

While $\sigma_\pm$ is the pauli matrices that describe a single $\frac{1}{2}$ spin which obeys the following anti-commutation relation:

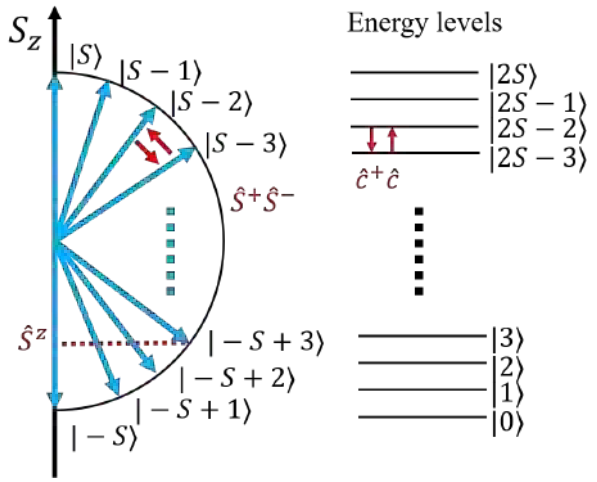

Figure 7: Energy levels of a collective spin system with N total spins (left) and the energy levels for magnons due to collective excitation of spins (right). The operator $\hat{S}^+$ and $\hat{S}^-$ act on the spin projection on z axis and $\hat{c}^+$ and $\hat{c}^-$ act on energy level of magnons.

$$\begin{aligned} \left\{\sigma_i, \sigma_i^\dagger\right\} &= 1 \\ \left\{\hat{S}_i, \hat{S}_i^\dagger\right\} &= 0 \end{aligned} \tag{41}$$

The Pauli spin operator is said to be "fermionic" and follows the Fermi–Dirac statistics and the collective spin operator is called "bosonic" and follows Bose–Einstein statistics because of the difference. This also explains the reason why electrons are fermions but magnons that formed by electrons are bosons. Here we show the proof of why. The collective operators are given as:

$$\begin{aligned} \hat{S}^2 \left|S, N\right\rangle &= S(S+1) \left|S, N\right\rangle \\ \hat{S}^z \left|S, N\right\rangle &= N \left|S, N\right\rangle \\ \hat{S}^+ \left|S, N\right\rangle &= \sqrt{(S+N+1)(S-N)} \left|S, N+1\right\rangle \end{aligned} \tag{42}$$

$|S, N\rangle$ represents the collective spin eigenstate of $\hat{S}^2$ and $\hat{S}^z$. The Hamiltonian of a insulating 1-D spin chain is given by Heisenberg model:

$$\hat{H}_m = -g\mu_B \sum_j^N \hat{B}\hat{S}_j - J \sum_j^N \hat{S}_j \cdot \hat{S}_{j+1} \tag{43}$$

Where $\mu_B = e\hbar/mc$ is the atomic moments, $g \approx 2$ is the gyromagnetic ratio and J is the ferromagnetic exchange constant. $\hat{B}$ is magnetic field usually assumed to be in the $\hat{z}$ direction. It is clear that the system can minimize its energy by having all the spins $\vec{S}$ align along the $\hat{z}$ direction at $T = 0$. To solve $\hat{H}$ at $T > 0$, we can express the Heisenberg operators $\hat{S}^+$ and $\hat{S}^-$ in terms of bosonic operators $\hat{c}_i$ and $\hat{c}_i^\dagger$, by using the Holstein-Primakoff transformation:

$$\begin{aligned}
\hat{S}_i^+ &= \hat{S}_i^x + i\hat{S}_i^y = \sqrt{2S}(1 - \frac{\hat{c}_i^\dagger \hat{c}_i}{2S})^{1/2}\hat{c}_i \approx \sqrt{2S}\hat{c}_i \\
\hat{S}_i^- &= \hat{S}_i^x - i\hat{S}_i^y = \hat{c}_i^\dagger\sqrt{2S}(1 - \frac{\hat{c}_i^\dagger \hat{c}_i}{2S})^{1/2} \approx \hat{c}_i^\dagger\sqrt{2S} \\
\hat{S}_i^z &= S - \hat{c}_i^\dagger \hat{c}_i
\end{aligned} \tag{44}$$

We have used the approximation of $\hat{c}_i^\dagger \hat{c}_i = N << 2S$ which means the procession angle of the spin is very small. Substituting the Holstein-Primakoff transformation into the Heisenberg model, the Hamiltonian of collective spin system can be rewrite as:

$$\begin{aligned}
\hat{H}_m &= -g\mu_B \sum_j^N \hat{B}\hat{S}_j - J\sum_j^N (\hat{S}_j^x \hat{S}_{j+1}^x + \hat{S}_j^y \hat{S}_{j+1}^y + \hat{S}_j^z \hat{S}_{j+1}^z) \\
&= -g\mu_B N B_z S - JNS^2 - JS\sum_j^N [\hat{c}_j \hat{c}_{j+1}^\dagger + \hat{c}_j^+ \hat{c}_{j+1} - 2\hat{c}_j^\dagger \hat{c}_j]
\end{aligned} \tag{45}$$

If we preform a Fourier transformation on the position space to momentum space, this means that the procession of local spin can be regard as the superposition of collective excitations of all spins. Applying the periodic boundary condition $K = 2b\pi/N$. The Hamiltonian can be write as:

$$\hat{H}_m = -g\mu_B N B_z S - JNS^2 - 2JSK^2 \sum_k \hat{a}_k^+ \hat{a}_k^- \tag{46}$$

Magnon result from collective excitation of spin wave. We can extract the Hamiltonian from the spin-wave(spin ensembles):

$$\hat{H}_{\text{magnon}} = \hbar \sum_k \omega_k \hat{a}^\dagger \hat{a} \tag{47}$$

2.3 Cavity Magnon Polariton

2.3.1 Coupled Oscillators

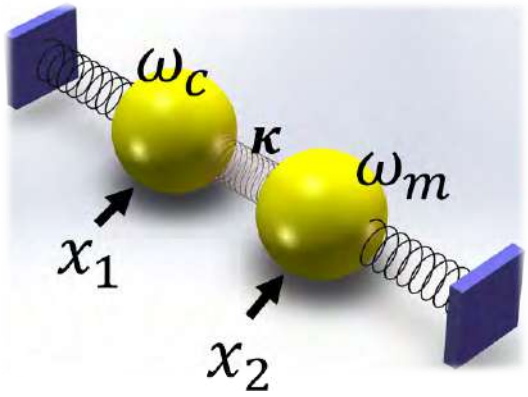

Figure 8: The coupled oscillator model, with x_1,x_2 representing the position and ω_c,ω_m as the intrinsic frequencies of the two oscillators. The damping terms α and β are depend on the spring loss of each oscillator. The coupling term κ is induced by the spring between two cavities.

Consider two damped spring oscillators with intrinsic frequency ω_c, ω_m (representing the cavity and magnon) coupled by a spring in between with a coupling strength κ. The driving force is only acting on the cavity oscillator because the microwave only excite the photon cavity. The equations of motion of coupled oscillators are easy to obtain as:

$$\begin{aligned} \ddot{x}_1 + \alpha\omega_c\dot{x}_1 + \omega_c^2 x_1 + \kappa\omega_c^2 x_2 &= f e^{i\omega t} \\ \ddot{x}_2 + \beta\omega_m\dot{x}_2 + \omega_m^2 x_2 + \kappa\omega_c^2 x_1 &= 0 \end{aligned} \tag{48}$$

Where x_1 and x_2 are the position of the oscillator 1 and 2, respectively, and have the solution form of $Ae^{i\omega t}$. The subscript c and m represent the amplitude of cavity mode and magnon mode. α and β are used to represent the damping parameter of the photon mode and magnon mode. We can rewrite the equation of motion in a matrix form:

$$\begin{pmatrix} \omega^2 - \omega_c^2 + i\omega_c\omega\alpha & -\kappa\omega_c^2 \\ -\kappa\omega_c^2 & \omega^2 - \omega_m^2 + i\omega\omega_m\beta \end{pmatrix} \begin{pmatrix} A_c \\ A_m \end{pmatrix} = \begin{pmatrix} f e^{i\omega t} \\ 0 \end{pmatrix} \tag{49}$$

Where the $fe^{i\omega t}$ term is the driving force acting on the cavity oscillator which represent the microwave sending to the photon cavity. The diagonal terms represent resonance of the cavity photons and magnon while the off-diagonal terms describe

the coupling between them. It can be obviously seen that in the limit of coupling term equals to zero, matrix model retards to two independent equations of motion that describe the cavity mode with a driving force and magnon modes without coupling.

Two complex roots can be obtained by solving the eigenvalue problems of this two-by-two matrix. The real parts give the anti-crossing dispersion relation and the imaginary parts give the linewidth exchange of the two modes. The two results can be used to explain the experiment data in CMP system which shows the Rabi frequency and linewidth exchange between two modes.

Eigenvalue of ω is given by the characteristic polynomial of the matrix:

$$det([M]) = (\omega^2 - \omega_c^2 + i\omega_c\omega\alpha)(\omega^2 - \omega_m^2 + i\omega\omega_m\beta) - \kappa^2\omega_c^4 = 0 \tag{50}$$

Assuming that the dispassion rates are usually far small than the resonant frequency $(\alpha, \beta << 1)$ and considering the cases near resonance and near coupling point($\omega \approx \omega_c \approx \omega_m$), we can use the approximation of $\omega+\omega_c \approx 2\omega_c$ and $\omega+\omega_m \approx 2\omega_c$. Eigenvalue of ω is given by the characteristic polynomial:

$$(\omega - \omega_c)(\omega - \omega_m) \cdot 4\omega_c^2 - \kappa^2\omega_c^4 = 0 \tag{51}$$

We can eliminate the $4\omega_c^2$ term by dividing it at both sides and expand the bracket to get:

$$\omega^2 - \omega(\omega_c + \omega_m) + \omega_c\omega_m - \frac{\kappa^2\omega^2}{4} = 0 \tag{52}$$

The roots which are eigenvalues can be obtained by using quadratic formula:

$$\omega_\pm = \frac{(\omega_c + \omega_m) \pm \sqrt{(\omega_c - \omega_m)^2 + \kappa^2\omega_c^2}}{2} \tag{53}$$

Where we have used detune as $\Delta = \omega_c - \omega_m$ and $\Omega = \sqrt{(\omega_c - \omega_m)^2 + \kappa^2\omega_c^2}$. By takeing the damping into consideration, solution of the eigenvalues $\omega_\pm$ gives resonant frequency anti-crossing (real part) and linewidth exchange (imaginary part) behaviors for CMP.

2.3.2 Quantum Hamiltonian

Consider a collective spin system mentioned in section 2.2.2 interacting with cavity photons. The Hamiltonian for a system of N two-level atoms of intrinsic

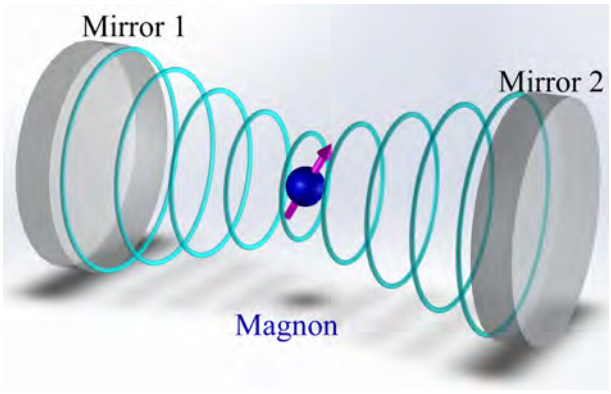

Figure 9: A sketch of spin-photon interaction. The sphere with an arrow at center is the collective spin system that has simplified as a giant spin. Photons between two mirrors forms standing waves that exchange energy with these spins.

frequency ω_0 interacting with a single mode cavity mode of frequency ω_c is

$$H = \hbar\omega_m \sum_i S_i^z + \hbar\omega_c a^\dagger a + \sum_i \hbar g(S_i^\dagger a + a^\dagger S_i) \tag{54}$$

where g is the coupling constant between the collective spin and cavity mode with the annihilation and creation operators a and $a^\dagger$. The Hamiltonian can be simplified as:

$$H = \hbar\omega_m S^z + \hbar\omega_c a^\dagger a + \hbar g(S^\dagger a + a^\dagger S_i) \tag{55}$$

The Hamiltonian matrix can be acquired through following, in which case the ground state is $|G\rangle = |N, -\frac{N}{2}, 0\rangle$ and here we use $|1\rangle = |N, -\frac{N}{2}, 1\rangle$ and $|2\rangle = |N, -\frac{N}{2}+1, 1\rangle$ as the degenerated excited states near $\omega_c = \omega_m$, the matrix elements are given as $\hat{H}_{ij} = \langle i|\,\hat{H}\,|j\rangle$.

$$\hat{H} = \begin{pmatrix} H_{11} & H_{12} \\ H_{21} & H_{22} \end{pmatrix} \tag{56}$$

where we have

$$\begin{aligned} H_{11} &= \langle 1|\hat{H}|1\rangle = \hbar\omega_m(-\frac{N}{2}) + \hbar\omega_c \\ H_{22} &= \langle 2|\hat{H}|2\rangle = \hbar\omega_m(-\frac{N}{2}+1) \\ H_{12} &= H_{21} = \langle 1|\hat{H}|2\rangle = -\sqrt{N}\hbar g \end{aligned}$$

Then the Hamiltonian matrix become:

$$H = \begin{pmatrix} -\frac{N}{2}\hbar\omega_m + h\omega_c & -\sqrt{N}\hbar g \\ -\sqrt{N}\hbar g & (-\frac{N}{2}+1)\hbar\omega_m \end{pmatrix} \tag{57}$$

Solving the characterize polynomial would give the eigenvalues which correspond the energy of CMP:

$$E_\pm = \frac{1}{2}((\hbar\omega_m(-N+1) + \hbar\omega_c) \pm \frac{1}{2}\hbar\sqrt{(\omega_c - \omega_m)^2 + 4Ng^2} \tag{58}$$

Use $\Omega = \sqrt{(\omega_c - \omega_m)^2/4 + Ng^2}$ as the generalized Rabi frequency, $\Omega_0 = \sqrt{Ng^2}$ as the Rabi frequency and detune $\Delta = \omega_m - \omega_c$. The energy can be rewrite as:

$$E_\pm = \hbar[(-\frac{N}{2}+1)\omega_m - \frac{\Delta}{2} \pm \Omega] \tag{59}$$

Solving normalized eigenvectors which are given as:

$$\vec{x}_+ = \begin{pmatrix} cos(\theta) \\ sin(\theta) \end{pmatrix} \qquad \vec{x}_- = \begin{pmatrix} -sin(\theta) \\ cos(\theta) \end{pmatrix} \tag{60}$$

with

$$\begin{aligned} tan(\theta) &= \frac{\Omega + \Delta/2}{\Omega_0} \\ sin(\theta) &= \sqrt{\frac{\Omega + \Delta/2}{2\Omega}} \\ cos(\theta) &= \sqrt{\frac{\Omega - \Delta/2}{2\Omega}} \end{aligned} \tag{61}$$

As you may notice, the result is very similar to the coupled oscillators model, in this quantum model, the damping effect is not considered. By constructing the damping Hamiltonian which has the same form of classical coupled oscillators we can get a similar result with the only difference is the definition of coupling strength and resonance for both magnons and cavity photons. If we consider the difference as different explanations on CMP coupling, the classical model is equivalent to this quantum model. Moreover, the eigenvector we solved in Eq.60 of mode $|\psi_+\rangle$ and $|\psi_-\rangle$ indicate that in-phase resonance have a higher energy and out-of-phase corresponds to lower energy in Fig.10(c)(d). As for detune equals zero ($\Delta = 0$), we have a frequency difference as $2\Omega_0 = 2\sqrt{4Ng^2}$, which is known as the Rabi frequency

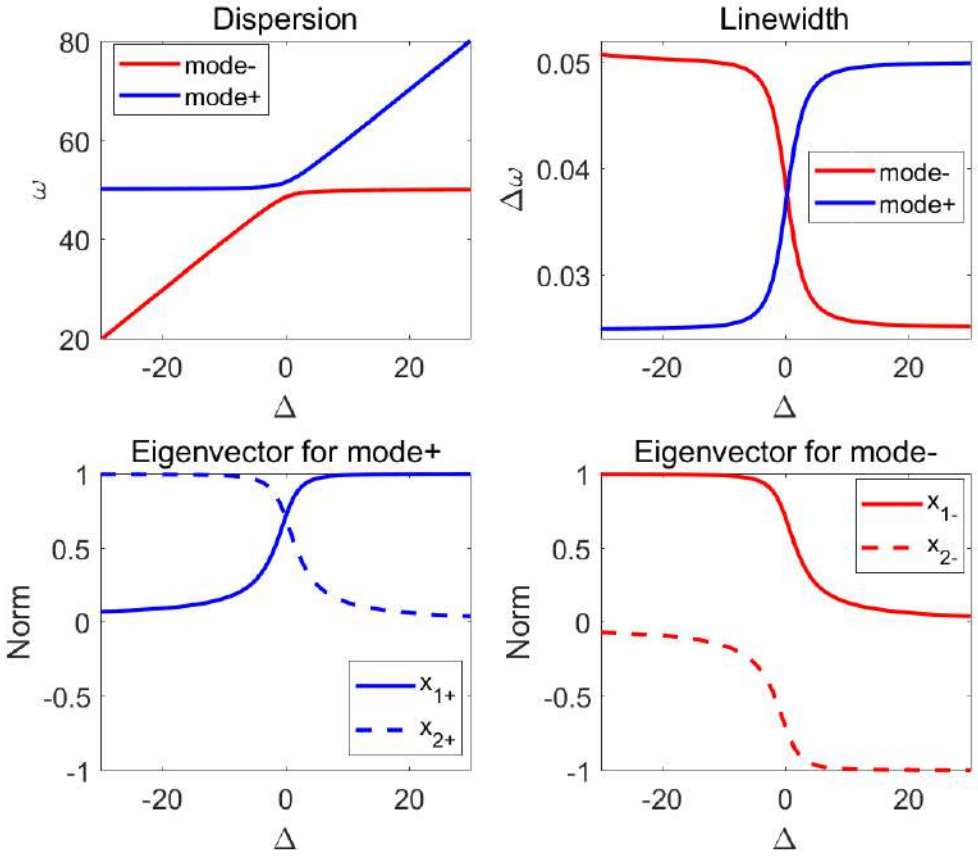

Figure 10: The properties of matrix model of CMP: (a) Dispersion relation with anti-crossing behavior. The center gap determine the coupling strength g at $\Delta = 0$. (b) Linewidth exchange of the two modes. As the linewidth evolves with magnetic field, one mode exchanged its linewidth with another. The two modes have a equal linewidth at $\Delta = 0$. (c) Eigenvector for mode+ (Eq.60 first term) plotted as a function of detune. where x_{1+}, x_{2+} are vector elements in $\vec{x}_+ = (x_{1+}, x_{2+})$. System oscillates in phase for higher energy mode. (d) Eigenvector for mode- (Eq.60 second term) plotted as a function of detune. x_{1-}, x_{2-} are vector elements in $\vec{x}_- = (x_{1-}, x_{2-})$. The system oscillates out of phase for lower energy mode.

In order to change the magnon-photon basis to CMP basis, we can diagonalize the Hamiltonian matrix:

$$\hat{H} = \begin{pmatrix} \hbar\omega_+ & 0 \\ 0 & \hbar\omega_- \end{pmatrix} \tag{62}$$

The eigenstates of the CMP system become as $|\psi_+\rangle$ and $|\psi_-\rangle$, and the corresponding eigenfrequencies are $\omega_\pm = \omega_c + \dfrac{\Delta}{2} \pm \Omega$. Then we have a new set of creation and

annihilation operators of CMP.

$$\begin{aligned} \hat{m}_{\pm}^{+} |G;0\rangle &= |\psi_{\pm}\rangle \\ \hat{m}_{\pm}^{-} |\psi_{\pm}\rangle &= |G;0\rangle \end{aligned} \tag{63}$$

And now the eigenstates becomes:

$$\begin{aligned} |E;0\rangle &= cos(\theta) |\psi_{+}\rangle + sin(\theta) |\psi_{-}\rangle \\ |G;1\rangle &= sin(\theta) |\psi_{+}\rangle + cos(\theta) |\psi_{-}\rangle \end{aligned} \tag{64}$$

This diagonalization technique is a purely mathematical treatment on CMP in which the spin-photon basis ($|\frac{N}{2} - \frac{N}{2}; 0\rangle, |\frac{N}{2} - \frac{N}{2}; 1\rangle, |\frac{N}{2} - \frac{N}{2} + 1; 0\rangle$) was changed to CMP basis ($|G\rangle, |\psi_{+}\rangle, |\psi_{-}\rangle$). These two basis describes the CMP equally well, however, the CMP basis will be convenient when we take active cavity photons into consideration.

2.3.3 Cavity Magnon Quintuplet

In this research, the mode of the active cavity was carefully designed to have the same frequency as the passive cavity. An additional coupling term between magnon and feedback photons appears because the presence of active cavity. Therefore, the Hamiltonian of the A-P-M devices is given by:

$$H = \hbar\omega_0 m^z + \hbar\omega_c \hat{p}^{\dagger}\hat{p} + \Omega_{PM}(\hat{m}^{+}\hat{p} + \hat{p}^{\dagger}\hat{m}^{-}) + \hbar\omega_c \hat{a}^{\dagger}\hat{a} + \Omega_{APM}(\hat{m}^{+}\hat{a} + \hat{a}^{+}\hat{m}) \tag{65}$$

Where $\hat{p}^{\dagger}$ and $\hat{p}$ are the creation and annihilation operators for P-cavity mode, $\hat{a}^{\dagger}$ and $\hat{a}$ describe the feedback photon of the A-cavity. Notice that Ω_{PM} and Ω_{APM} are coupling strength for P-M coupling and A-P-M coupling, respectively. In this case, we consider the collective spin state $|(\frac{N}{2}, -\frac{N}{2} + m)\rangle$ that involves m spin excitations, now the two states $|(\frac{N}{2}, -\frac{N}{2} + m); 0\rangle$ and $|(\frac{N}{2}, -\frac{N}{2} + m - 1); 1\rangle$ exchange energy with each other. The coupling between the active photon cavity and the magnon is given by:

$$\begin{aligned} \Omega_{APM} &= \frac{1}{m} \langle \frac{N}{2}, -\frac{N}{2} + m; 0 | \, g_0(\hat{m}^{+}\hat{a} + \hat{a}^{+}\hat{m}) \, | \frac{N}{2}, -\frac{N}{2} + m - 1; 1 \rangle \\ &= \sqrt{\frac{N - m + 1}{m}} g_0 \end{aligned} \tag{66}$$

Where g_0 is the vacuum Rabi frequency of a single spin interact with cavity photons. In Eq.66, we treat this system with N spins and m spin excitations as a quantum-

mechanical system. In the limit of linear spin dynamic regime with $m << N$, the coupling strength becomes $\sqrt{\frac{N}{m}}g_0 \approx \frac{\Omega_0}{\sqrt{m}}$. Because m spin excitations coupled with the feedback cavity photons, these dynamic effects the coupling strength changes with the number of feedback photons. Transfer the spin-photon basis to CMP basis, the Hamiltonian for the A-P-M device can be rewrite as:

$$\frac{\hat{H}}{\hbar} = \omega_+ \hat{m}_+^z + \omega_- \hat{m}_-^z + \omega_c \hat{a}^\dagger \hat{a} + \Omega_{APM}(\hat{m}^+ \hat{a} + \hat{a}^+ \hat{m}) \tag{67}$$

Recall that the transferred states are from the superposition of the two degenerated states follows relation $|\psi_\pm\rangle = c_\pm |E;0\rangle \pm c_\mp |G,1\rangle$ where $c_+ = \sqrt{(\Omega + \Delta/2)/2\Omega}$ and $c_- = \sqrt{(\Omega - \Delta/2)/2\Omega}$ represent the amplitude of two excited states in CMP system with $\Omega = \sqrt{\Omega_0^2 + (\Delta/2)^2}$. Collective excitations leads to the CMP modes appearing at $\omega_\pm = \omega_c + \Delta/2 \pm \Omega$ in CMP basis, and it is easy to get:

$$\begin{aligned} |E;0\rangle &= c_+ |\psi_+\rangle + c_- |\psi_-\rangle \\ |G;1\rangle &= c_- |\psi_-\rangle - c_+ |\psi_+\rangle \end{aligned} \tag{68}$$

Substitute this into Eq.65 to get a set of new operators for $|\psi_\pm\rangle$:

$$\begin{aligned} \hat{m}^+ &= |E;0\rangle \langle G;0| = c_+ |\psi_+\rangle \langle G;0| + c_- |\psi_-\rangle \langle G;0| \\ \hat{m}^- &= |G;0\rangle \langle E;0| = c_+ |G;0\rangle \langle \psi_+| + c_- |G;0\rangle \langle \psi_-| \end{aligned} \tag{69}$$

where $\hat{m}^+$ excites the system from ground state to $|\psi_+\rangle$ while $\hat{m}^-$ excites system from ground state to $|\psi_-\rangle$. By using the new set operators, we can reorganize the coupling term in Eq.67:

$$\hat{m}^+ \hat{a} + \hat{a}^\dagger \hat{m}^- = c_+(\hat{m}_+^+ \hat{a} + \hat{a}^\dagger \hat{m}_+^-) + c_-(\hat{m}_-^+ + \hat{a}^\dagger \hat{m}_-^-) \tag{70}$$

Therefore, Hamiltonian of A-P-M device in the CMP space that defined by two eigenstates of CMP can be acquired by substitute Eq.70 into Eq.67:

$$\frac{\hat{H}}{\hbar} = \omega_+ \hat{m}_+^z + \omega_- \hat{m}_-^z + \omega_c \hat{a}^\dagger \hat{a} + \frac{c_+ \Omega_0}{\sqrt{m}}(\hat{m}_+^+ \hat{a} + \hat{a}^\dagger \hat{m}_+^-) + \frac{c_- \Omega_0}{\sqrt{m}}(\hat{m}_-^+ \hat{a} + \hat{a}^\dagger \hat{m}_-^-) \tag{71}$$

First we consider $|\psi_+\rangle$ and $|G\rangle$ couples with active cavity energy level $|n\rangle$, there are two sets of degenerated states we need to consider. We note $|1e\rangle = |\psi_+, n\rangle$, $|2e\rangle = |G, n+1\rangle$ and $|1g\rangle = |G, n\rangle$, $|2g\rangle = |\psi_+, n-1\rangle$ as the degenerate states in excited state and ground states (see Fig.11) ,respectively. Then we apply the

same trick in section 2.3.2 where the Eq.56 become two sets. Because this scenario only involves $|\psi_+\rangle$, we only need to consider the first coupling term. Hence, for $\hat{H}_+ = \frac{c_+\Omega_0}{\sqrt{m}}(\hat{m}_+^+\hat{a} + \hat{a}^\dagger\hat{m}_+^-)$ it is easy to find that:

$$\begin{aligned} H_{11g} = H_{22g} = H_{11e} = H_{22e} = 0 \quad &\text{for diagonal term} \\ H_{21g} = H_{21g} = \frac{c_+\Omega_0\sqrt{n}}{\sqrt{m}} = c_+\Omega_0 f \quad &\text{for off-diagonal term} \\ H_{21e} = H_{21e} = \frac{c_+\Omega_0\sqrt{n+1}}{\sqrt{m}} \approx c_+\Omega_0 f \end{aligned} \tag{72}$$

Here we have defined a feedback factor f by using the n and m, where n is the energy level of the feedback cavity given by $n = \hat{a}\hat{a}^\dagger$:

$$f = \sqrt{\frac{n}{m}} \tag{73}$$

The matrix Hamiltonian for $|\psi_+\rangle$ and $|G\rangle$ states for CMP and feedback photons are given by:

$$[\hat{H}_{g+}] = \begin{pmatrix} n\omega_c & c_+\Omega_0 f \\ c_+\Omega_0 f & \omega_+ + (n-1)\omega_c \end{pmatrix} \qquad [\hat{H}_{e+}] = \begin{pmatrix} \omega_+ + n\omega_c & c_+\Omega_0 f \\ c_+\Omega_0 f & (n+1)\omega_c \end{pmatrix} \tag{74}$$

Solving the eigenvalue we found two sets of energy splitting, one for ground state and the other for excited state:

$$\begin{aligned} \hat{E}_{g+} &= (n - \frac{1}{2})\hbar\omega_c + \frac{1}{2}\hbar\omega_+ \pm \frac{\hbar}{2}\sqrt{\Omega + \frac{\Delta}{2})^2 + \frac{2(f\Omega_0)^2(\Omega + \Delta/2)}{\Omega}} \\ \hat{E}_{e+} &= (n + \frac{1}{2})\hbar\omega_c + \frac{1}{2}\hbar\omega_+ \pm \frac{\hbar}{2}\sqrt{\Omega + \frac{\Delta}{2})^2 + \frac{2(f\Omega_0)^2(\Omega + \Delta/2)}{\Omega}} \end{aligned} \tag{75}$$

If we perform the same trick on $|\psi_-\rangle$ state of CMP we can retrieve the set of solution for $\hat{H}_-$ and $\hat{E}_{g-}$, $\hat{E}_{e-}$.

$$\begin{aligned} \hat{E}_{g-} &= (n - \frac{1}{2})\hbar\omega_c + \frac{1}{2}\hbar\omega_+ \pm \frac{\hbar}{2}\sqrt{\Omega - \frac{\Delta}{2})^2 + \frac{2(f\Omega_0)^2(\Omega - \Delta/2)}{\Omega}} \\ \hat{E}_{e-} &= (n + \frac{1}{2})\hbar\omega_c + \frac{1}{2}\hbar\omega_+ \pm \frac{\hbar}{2}\sqrt{\Omega - \frac{\Delta}{2})^2 + \frac{2(f\Omega_0)^2(\Omega - \Delta/2)}{\Omega}} \end{aligned} \tag{76}$$

From the energy level diagram (shown in Fig.11) it is easy to know the there are eight

possible emissions in which four have exactly same energy. This energy splitting gives five CMP modes (ω_c, $\omega_c \pm \Omega+$,$\omega_c \pm \Omega_-$) on emission spectrum which is named as "Cavity Magnon Quintuplet", when $\Delta = 0$ we can observe a "Magnon Triplet" due to $\Omega_+ = \Omega_-$. The Rabi frequencies of these CMP system is obtained as:

$$\Omega_\pm = \sqrt{(\Omega \pm \frac{\Delta}{2})^2 + \frac{2(f\Omega_0)^2(\Omega \pm \frac{\Delta}{2})}{\Omega}} \tag{77}$$

The Rabi frequency $\Omega_\pm$ is related with a factor $\sqrt{m}$ (in f) in denominator that relates with the number of CMPs in this system and a factor in $\sqrt{n}$ in numerator that relates with the number of feedback photons that can be controlled by voltage. Based on these relations, there are two approaches to tune the feedback factor f. One way is change the value of m, the other way is change the number of feedback photons.

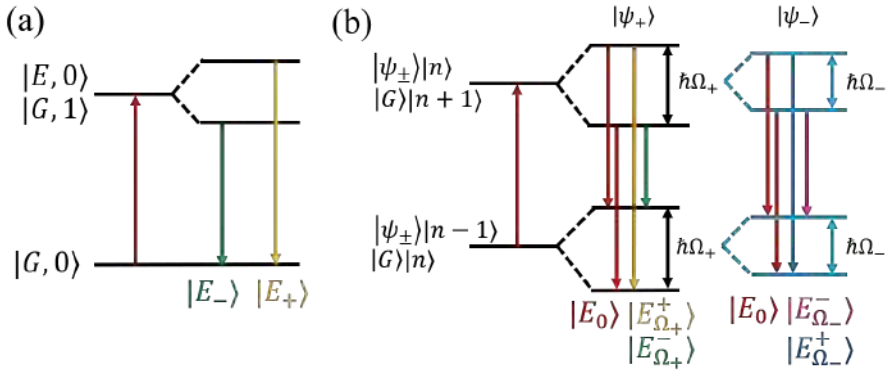

Figure 11: Energy level split of the system (a) Sketch of energy levels for normal anti-crossing, on the left is the energy level without interaction at $\Delta = 0$ and on the right is the energy splitting due to coupling. (b) Schematic of energy levels for A-P-M devices. Four red arrow corresponds to the decays with same energy $\hbar\omega_c$. At $\Delta = 0$, they produce the magnon triplet with $\Omega_+ = \Omega_-$. At $\Delta \neq 0$, they produce the magnon quintuplet with $\Omega_+ \neq \Omega_-$

3 Experiment Methods

As described previously, the generation of CMP is being extensively investigated and has many potential practical applications [15, 20, 22–27]. It has been demonstrated that this coupling offers a promising approach to develop long-lifetime broadband, multi-mode quantum memories [31], quantum repeaters [31] and quantum transducers that could coherently exchange information between different quantum systems [32]. However, the previous experiment performed to demonstrate CMP has limitations in terms of adapting them into practical applications. Cavity with sealed conducting walls that create an ideal boundary condition for resonance which have relative low loss and produce a high Q factor. This usually means they require complex mechanical operates to change the position of magnon or samples [26] in order to vary the properties of the system. Therefore, development of an active planar tunable cavity whose dispassion rate and coupling strength can be easily and continuously tuned would bring great conveniences and a new perspective to study CMP. Such a cavity would also help in easier integration of this photon-magnon coupling system to on-chip devices for advanced spintronics applications.

3.1 Cavity Design

A very important parameter of a resonator is its quality factor Q. It can be defined as the ratio of the energy stored in the resonator and the energy required to maintain a constant amplitude of resonance under the resonant frequency ω_0 :

$$Q = 2\pi \times \frac{\text{Energy Stored}}{\text{Energy loss per cycle}} = \frac{\omega_0}{\Delta\omega} \tag{78}$$

Where $\Delta\omega$ is the full width at half maximum(FWHM) or the resonant linewidth of the resonance, and this argument is only true when the Q factor is large enough meaning the resonator become less damped. Q factor is simply a measure of resonator loss.

3.1.1 Microstrip resonator cavity

Microstrip resonators are a kind of electric circuits fabricated on PCB board to convey microwave frequency signals. It consists of a conducting strip separated from a ground plane by a dielectric layer known as the substrate. There are four common designs for microstrip cavity that shown in shown in Fig.12.

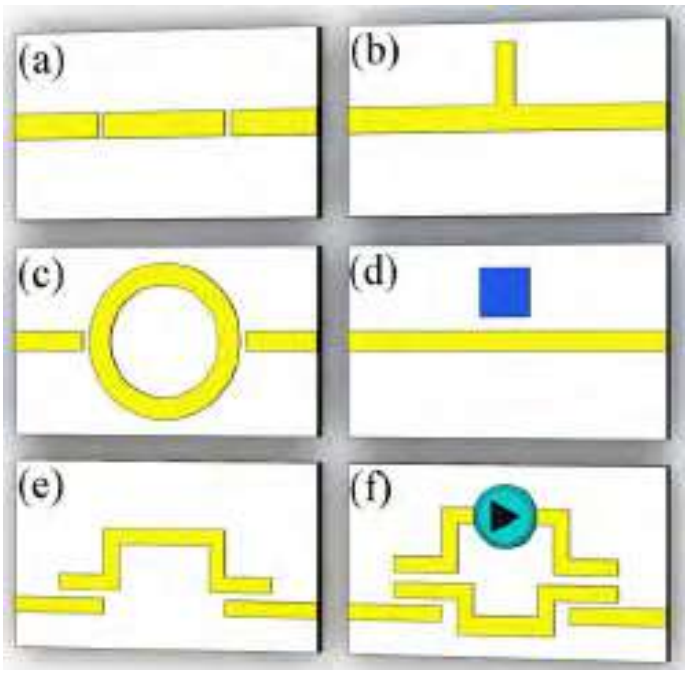

Figure 12: (a-d) Four common designs of microstrip resonator with (a) Open-end resonator. (b) Stub resonator.(c) Ring resonator. (d) Dielectric resonator with the square object (blue) as dielectric. (e) modified open-end resonator was chosen as the active photon cavity. (f) A-P resonator design we used in this experiment, with a amplifying circuit integrated in the top which formed a feedback loop in this case.

The Open-end resonator, Stub resonator(also known as cut-wire), ring resonator and dielectric resonator are the four common designs of microwave cavities. The resonator condition is given as following:

$$L = n \cdot (\frac{1}{2}) \cdot \lambda_g; \quad n = 1, 2, 3... \qquad \text{For Open-end resonator}$$

$$L = n \cdot (\frac{1}{4}) \cdot \lambda_g; \quad n = 1, 2, 3... \qquad \text{For open stub resonator}$$

$$2\pi R = n \cdot \lambda_g; \qquad n = 1, 2, 3... \qquad \text{For Ring resonator}$$

Where λ_g is the wavelength that relate to resonant frequency and effective dielectric constant. For open-end and ring resonator, the transmission spectra have peaks because signal can be transmitted if it is in resonance. The microwave would be blocked because the metal part is not directly connected while off-resonance. For stub resonator, a dip will occur near resonance because the reflected wave from the end stub cancels incoming wave and transparent for microwave while off resonance.

3.1.2 Feedback cavity

The resonator design in our study is open-end resonator with a relatively long feed length. The design of "Ω" shaped resonator brings a great convenience to integrate the amplifying circuit of the feedback loop. The structure of the feedback cavity is schematically shown in Fig.13. We first use a planar passive cavity (P) with a mode frequency ω_c to couple photons with the magnons (M) in a ferromagnetic insulator YIG. This "P-M" design is used in most of the previous work. The key innovation of this experiment is the design and implementation of an active cavity (A) which contains a microwave amplifier with bias voltage (V) controlled gain (G_n). The two cavities (A and P) are carefully designed to have the same mode frequency. This kind of cavity setup is called A-P-M design(system).

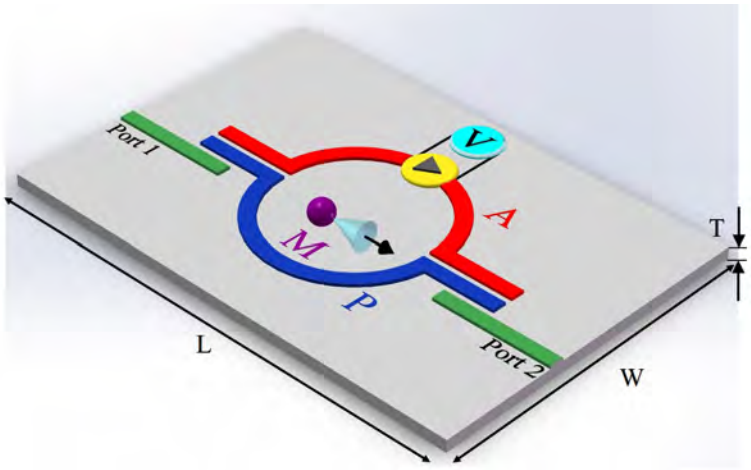

Figure 13: A-P-M device configuration, the green lines (marked with Port 1 and Port 2) are feed lines that connect to VNA. Blue part marked with "P" is the passive cavity while letter "A" colored red is the active cavity with a amplifying circuit in orange with a triangle. A YIG sphere marked "M" in purple was placed above the P cavity. Bright blue part with "V" is the voltage source that supply the bias voltage for amplifying circuit. The magnetic field points to x direction.

As shown in Figure.13, the geometry of the active microstrip cavity has a length L = 5.0cm, width W = 3.0cm and thickness T = 1.55mm.

3.2 Experiment Setup

The main components of the measurement setup are a Agilent N5230C vector network analyser(VNA) to measure the transmission and reflection of the two port system, an active cavity fabricated from RT/duroid 5880 Laminates boards with

dielectric constant 2.20 and a loss tangent 0.0009, two KORAD KA3005D digital-control DC power supplies that provide the bias voltage for the feedback loop, a YIG sphere with 1.0 mm diameter as the collective spin system for interaction, a 3-D stage with a sample holder that can change the position of the YIG sphere, and an electromagnet provide the static magnetic field. The general setup is shown in Figure.14.

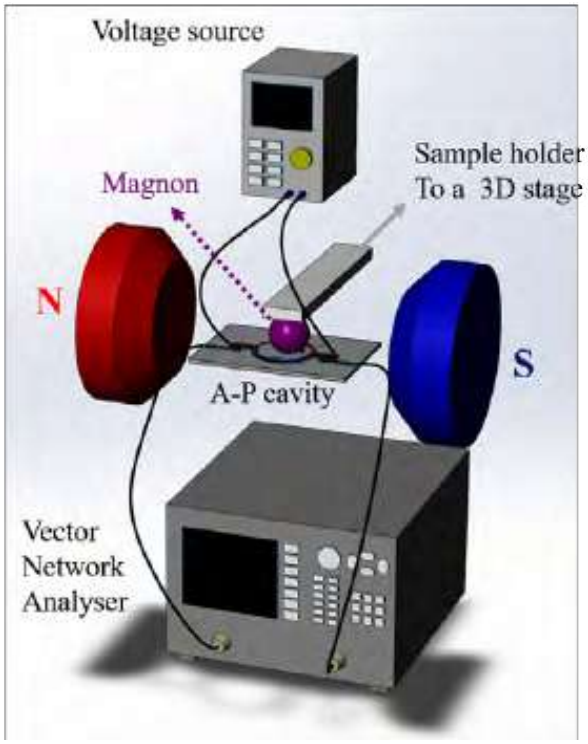

Figure 14: Experiment setup. A-P cavity was placed between two electromagnets (marked N red and S blue) and fixed. Magnon (1mm diameter YIG sphere) was placed in a sample holder made by Teflon which is connected to a X-Y-Z stage. Two feed lines were connected to Vector Network Analyser which can measure the transmission S_{21} directly and the voltage source provides the bias voltage for active cavity.

The static magnetic field to magnetize the YIG sphere is provided by an electromagnet with a Helmholtz coil, a uniformly distributed is formed near the center of the coil cylinder. Certain ferromagnetic material with a high magnetic permeability was placed in center of the coil in order to enhance the magnetic field. Vector Network Analyser(VNA) is a type of instruments that can measure network parameters of electrical network. VNA is commonly used in measuring S-parameters to acquire the reflectance and transmission which can characterize the desired systems. Major contents in the VNA circuit are a microwave signal generator, a test set and a re-

ceiver. Two power supplies were used to provide bias voltage for the transistor in feedback circuit. The X-Y-Z stage we used to change the position of the YIG sphere is from ATAGO optical works CO.LTD connect with a sample holder made by teflon. The data collection was automated by LabVIEW programs and data analysis is in MATLAB.

4 Experiment Results

In this section, we present experiment results which were divided into three parts. First we characterize the properties of active cavity by setting the magnetic field equal to zero. Second the YIG sphere was set to a fixed position. By tuning the voltage, the coupling regime and the coupling strength of CMP can be controlled. Third we set the voltage to 7V (the transistor is fully functional under that voltage) and tune the position of the YIG sphere. The transmission S_{21} of this system using input-output theory is given by [26]:

$$|S_{21}| = \left| \frac{A \cdot \kappa/2}{\omega - \omega_c + i\frac{\gamma_c}{2} - \frac{g^2}{\omega - \omega_m + i\frac{\gamma_m}{2}}} \right| \tag{79}$$

Where g, γ_c and γ_m has the same definition as in Fig.1. A is the amplitude of the resonance, and κ is the coupling constant result from port 1 and 2. This expression of S_{21} is used to fit the experiment spectra.

4.1 Characterize Active cavity

First the properties of active cavity was determined and shown in Fig.15. The experiment setup is the same as Fig.14 with magnetic field turned off (H field = 0 Gs). By sweeping the bias voltage on feedback loop from 0 to 7 V, a spectrum mapping is shown in Fig.15(a), there is a turning point that we call "turn on" point of the active cavity near 2.4V above which voltage the amplify will be triggered on. The Q factor that calculated from fitting lorentz lineshape of the spectra can reach up to 10^5 and a jump near 2.4V is observed. The existence of the "turn on" point is believed result from the properties of PN junction of transistor in feedback loop. S_{21} is greater than one shown in Fig.15(e) which means the output is stronger than input because microwave source in VNA is not only energy source but also the external

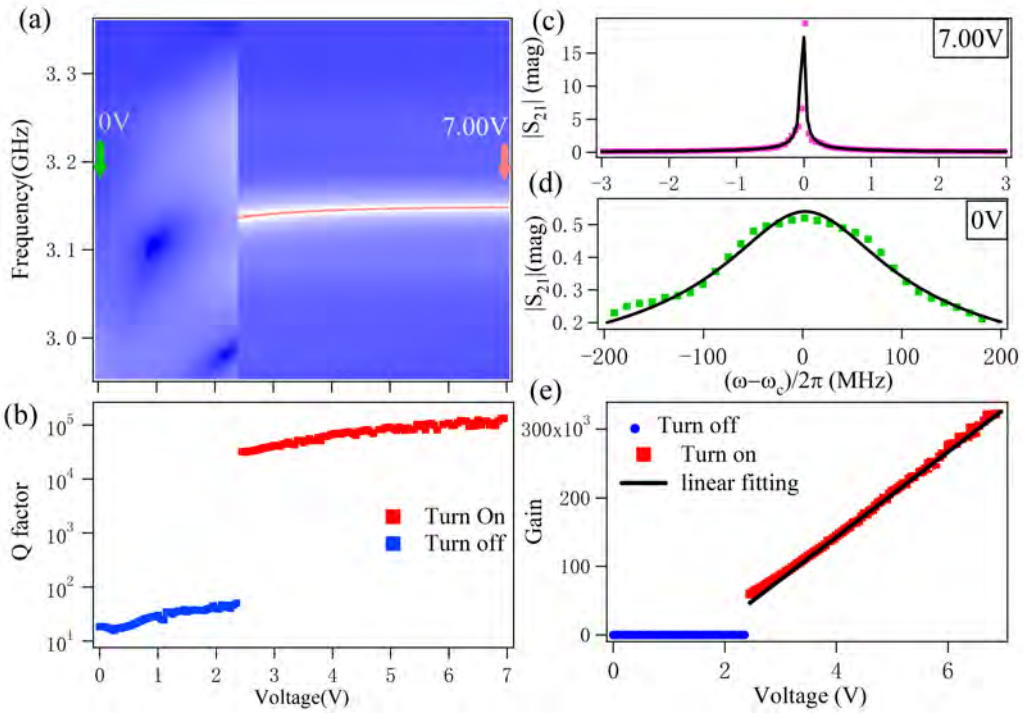

Figure 15: The properties of active cavity: (a) spectrum mapping of the active cavity as function of applied voltage on feedback circuit, a turn-on point can be clearly seen on the mapping. (b) The Q factor v.s. bias voltage which increased almost 3 order of magnitude, data acquired by using spectrum fitting.(c)(d) Typical spectrum(markers) and fitting results(black lines) at bias voltage equal to 0V and 7V, respectively. (e) Gain of the amplifying circuit v.s. voltage.

voltage source of feedback loop. It is reasonable that small signal with certain narrow band frequency is amplified and re-injected into system. Two typical spectrums and their fitting was given in Fig.15(c)(d), from fit curve the Q factor was determined to be $Q = 18$ at V=0 V and $Q = 1.32 \times 10^5$ at V = 7.0 V which indicate the active cavity we fabricated has the capability to achieve very high Q resonance and have a relative large tuneable range. Gain of the amplifying circuit was calculated by using the maximum signal strength of different bias voltage over the signal strength at V = 0 V. As we can see, the gain has approximately a linear relation as a function of applied voltage after the amplifying circuit being turned on:

$$G_n = (5.75 \cdot V - 8.40) \times 10^4 \tag{80}$$

Because of these properties, we can tune the damping of the microwave cavity by simply tuning the bias voltage.

4.2 Magnetically Induced Transparency

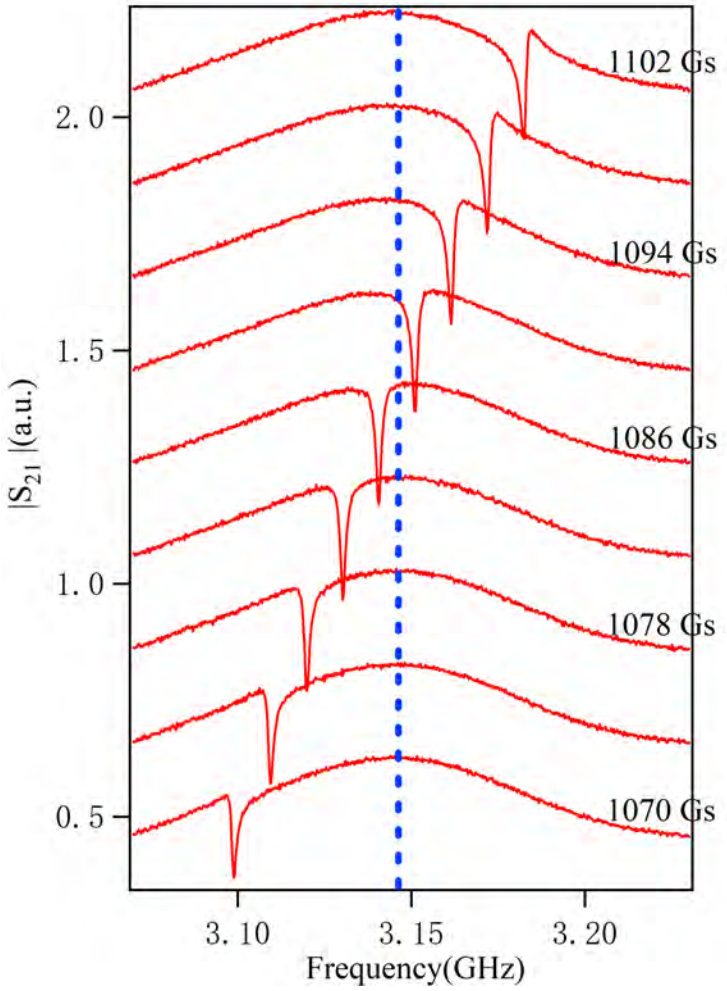

Figure 16: The waterfall plot of MIT, magnetic field is increasing from bottom to top. A sharp FMR passing through a wide cavity mode and creating a "transparent" window near resonance.

Magnetically induced transparency(MIT) which is the magnetic analog of the electromagnetically induced transparency(EIT). To achieve this regime, the damping of the microwave photon cavity needs to be dominates($\kappa_m < g < \kappa_a$) and the avoided crossing feature in the measured spectrum disappeared. A medium transparent window result from FMR passing through the wide cavity mode can be seen from spectrum as presented in the waterfall plot shown in Fig.16.

In this experiment, the feedback bias voltage was set to zero so that there is no signal being amplified. By sweeping the external magnetic field, an transparent window passes through the broad microwave cavity resonance can be seen on spectrum

mapping in Fig.17(a). From the measured data, we first determined the dispersion in Fig.17(b) and linewidth exchanges in Fig.17(d), the markers are fitting results and curves are matrix model calculation. The corresponding dissipation rates and the coupling strength are fitted at detune equal to zero as $\gamma_a/2\pi = 121.2$ MHz, $\gamma_m/2\pi = 0.85$ MHz and $g/2\pi = 6.46$ MHz shown in Fig.17(c) , corresponding to a cooperativity value of $C = (g/\gamma_a)(g/\gamma_m) = 0.4$ which indicate this is not a coherent interaction for this specific device configuration.

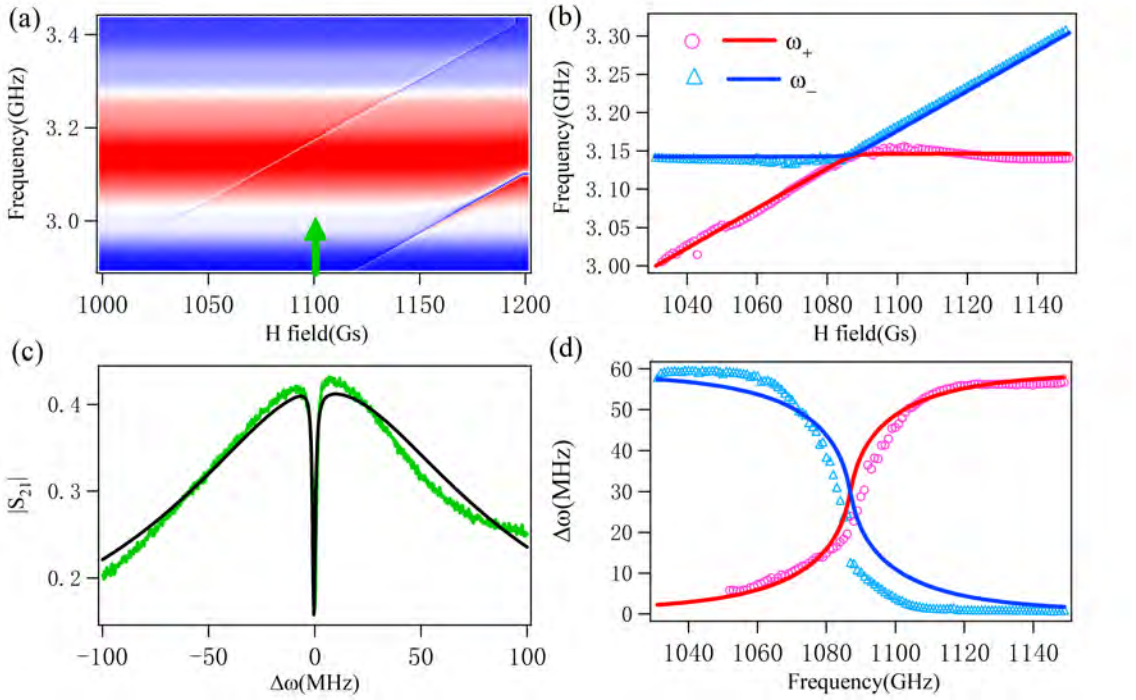

Figure 17: The fitting plot of MIT (a) Spectrum mapping of MIT (b) Resonant peak from fitting result(marks) and matrix calculation(solid lines). (c) Spectrum at detune equal to zero, light green curve is measured data and black curve is fitted data. (d) Linewidth from fitting(marks) and calculation(solid lines), this shows the linewidth exchange.

EIT is firstly found as being a quantum interference effect that permits the propagation of light through an otherwise opaque atomic medium [34]. Studying MIT would extend the concept of EIT and allow us have a better understanding of energy exchange between cavity photons and magnon. With the advancement of EIT physics extending to MIT, EIT like behavior provided the opportunity for narrow band transmission and light slowing effect at room temperature [35].

4.3 Strong Coupling

The strong coupling implies coherent dynamics between the photon and the magnon, such as avoided crossing in dispersion and Rabi-like oscillations in time domain. Two degenerated mode repelling each other near resonance in spectrum mapping (Fig.18(a)) and the fitting result as well as the calculation of matrix model is shown in Fig.18(b) which indicate a good agreement. In order to achieve this coupling regime, the coupling of CMP needs to be greater than damping of both cavity and magnon ($g > \gamma_m, \gamma_c$). The bias voltage was set to 0.64 V which apparently blow the tuning point 2.4V shown in Fig.15(a,b). We can clearly see a avoided crossing from spectrum mapping given in Fig.18(a). In most of previous works, the damping of photon cavity is a constant under different magnetic field. On the contrary, the damping rate of the microwave cavity in our device setup is changing under different applied H fields. At low H field blow 1045 Gs, the cavity mode is not visible and when H field is over 1050 Gs, the cavity mode become clear on spectrum. The dissipation rates was determined as $\gamma_a/2\pi = 20.3$ MHz at 1040 Gs and $\gamma_a/2\pi = 1.2$ MHz at 1110 Gs. The area of the resonance peak has increased which means the feedback loop is gradually being tuned on during this process. Further study is need to determine weather this phenomenon is given rise by presence of magnon or simply the magnetic field.

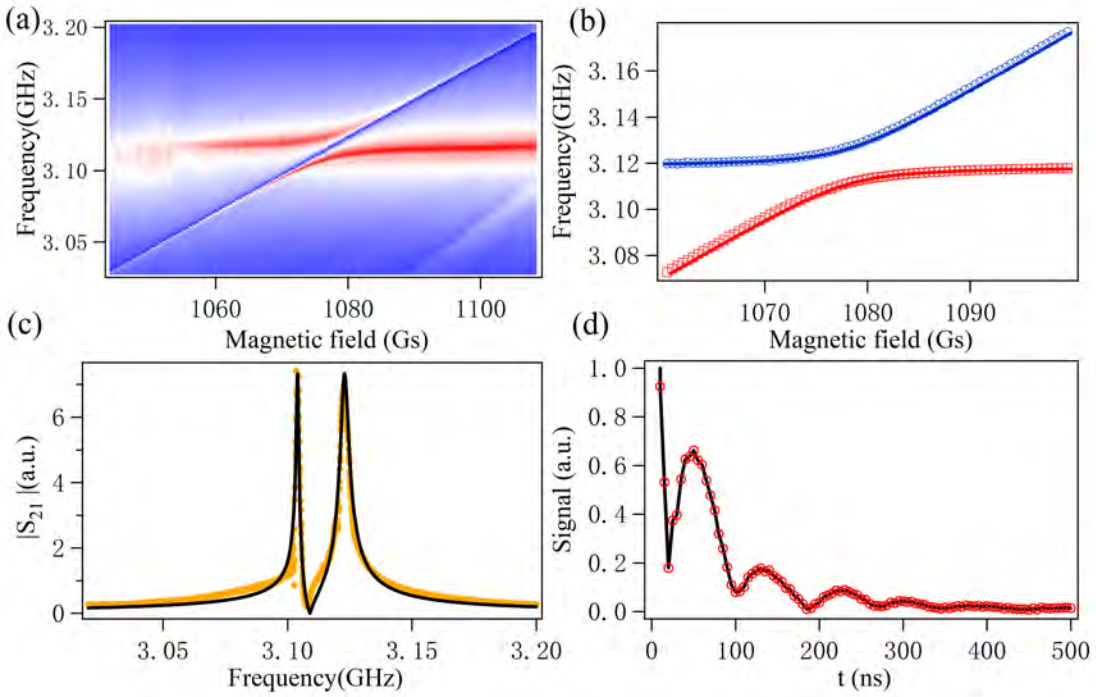

Figure 18: Characterize strong coupling in A-P-M device (a) Spectrum mapping of strong coupling. (b) Resonant peak from fitting result(marks) and matrix calculation(solid lines). (c) Spectrum at detune equal to zero, the marker in orange is experiment data and the black curve is the fitting result using Eq.79. (d) Inverse fast Fourier transform of experiment data in (c), from the time domain signal we can see the Rabi oscillation with dispassion.

The coupling strength at $\Delta = 0$ was determined to be $g/2\pi = 6.5$ MHz, and damping to be $\gamma_c/2\pi = 4.0$ MHz and $\gamma_m/2\pi = 0.33$ MHz (Fig.18(c)). The cooperativity has risen to $C \approx 32$. The time domain signal was obtained by using inverse fast Fourier transformation (iFFT) on spectrum at $\Delta = 0$ (shown in Fig.18(d)) whose oscillation period corresponds to coupling strength g given by $\frac{\pi}{g} = 76.9$ ns which corresponds to the time period around 80 ns. Clearly, the cavity energy experiences periodic oscillation aside from the exponential decay, demonstrating the coherent energy exchange between photon and magnon. Therefore, we have shown that by simply tuning the voltage which mean increase the number of feedback photons the coupling strength has been changed.

Strong coupling has been proved to have many applications in information processing such as transducers that can interconnect different systems such as photonics, mechanics, and microwave circuits [26] and device for quantum control and measurement of the magnon [32]. Strong coupling in this feedback-coupled cavity brings potential applications for information processing in spintronics.

4.4 Cavity Magnon Quintuplet

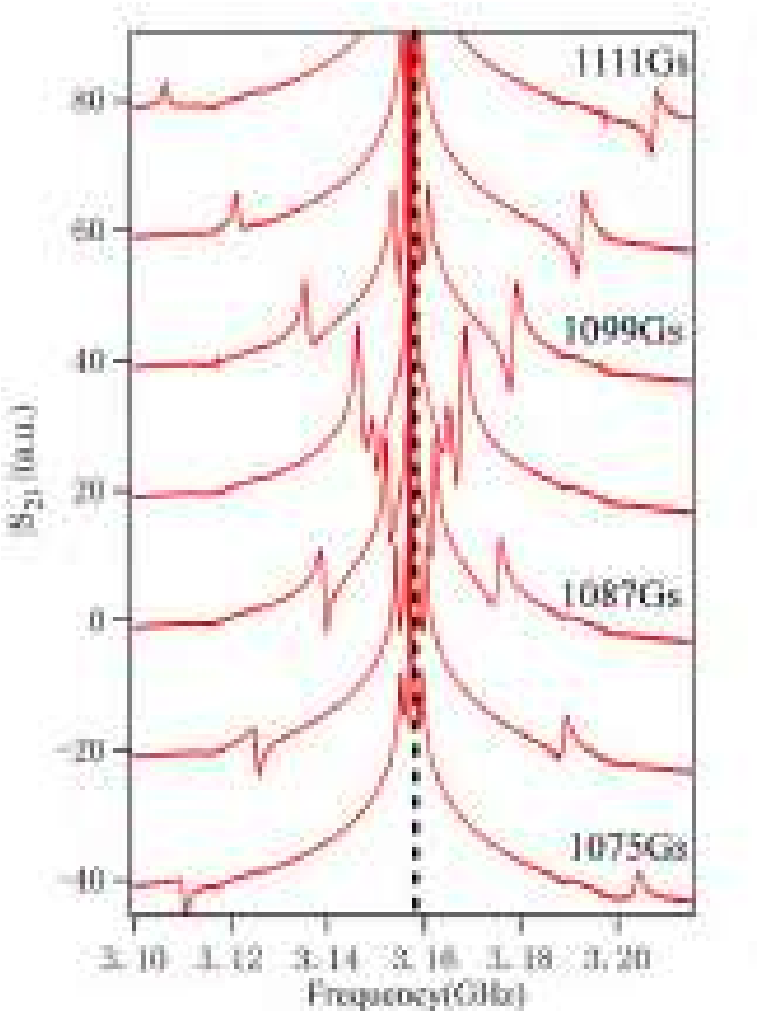

Figure 19: The waterfall plot of magnon quintuplet, magnetic field is increasing up directional. Five modes can be observed which can be well explained by the theory we introduced.

When the bias voltage was set as V = 7 V with the same YIG position as previous experiments. The feedback loop get fully "turned on" and the system has reached to a new coupling regime. Waterfall plot of spectra was shown in Fig.19 with the magnetic field increased from bottom to top, it is clear that each spectrum have five resonance modes evolving with the external magnetic field. This coupling regime with five modes is named as "cavity magnon quintuplet".

Spectrum mapping is given in Fig.20(a) where the dispersion relation with fitting and theory model calculation (section 2.3.3) is shown in Fig.20(b) which is in excellent agreement. Fig.20(c) gives the spectrum at $\Delta = 0$ where magnon quintuplet retards

to magnon triplet due to $\Omega_- = \Omega_+$. The linewidth of five different mode was fitted as Fig.20(d) in which we can observe a difference in magnitude. The center mode (at ω_c) corresponding to the feedback cavity has a very narrow linewidth and independent of external field while the other modes corresponds to CMPs (at $\omega_c \pm \Omega_-$ and $\omega_c \pm \Omega_+$) have a relative large linewidth and they still present exchange properties similar to the matrix model.

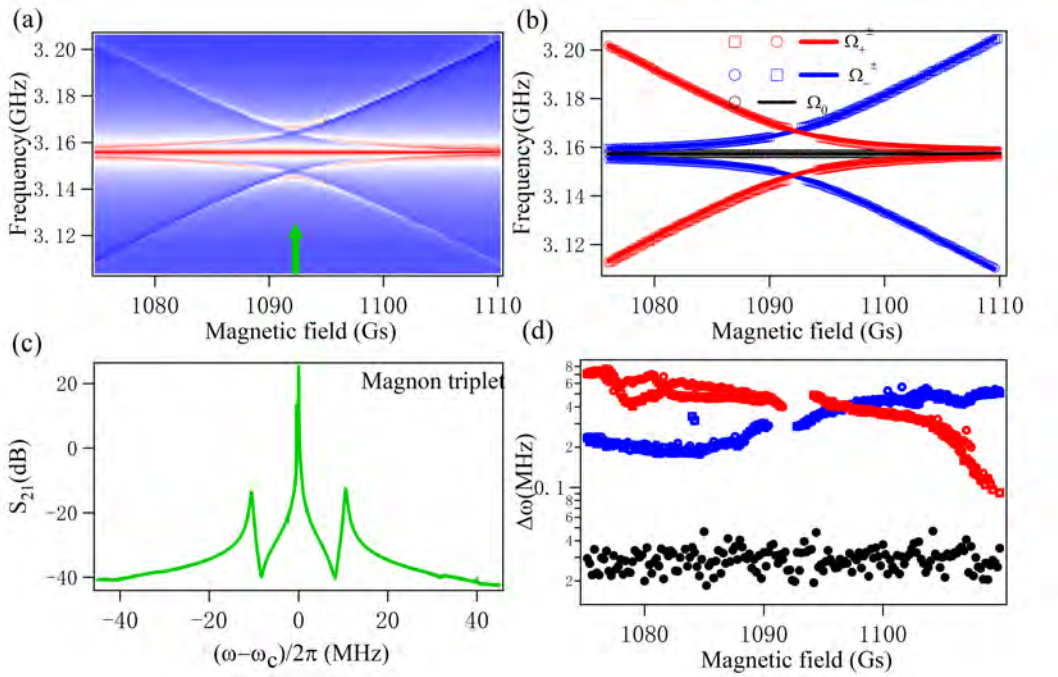

Figure 20: Magnon quintuplet (a) Spectrum mapping with frequency in y axis and H field as x axis, we can clearly see five modes when $\Delta \neq 0$ and three modes in center near resonance. (b) Peak positions read out from measured S_{21} (markers) and calculation result (lines) using model in Eq.77. (c) Spectrum at $\Delta = 0$ which gives a magnon triplet due to Ω_- and Ω_+ degenerate. (d) The linewidth of each mode use fitting, the red marks and blue marks represents side modes are black corresponds to the central mode.

4.5 Voltage Dependent Feedback

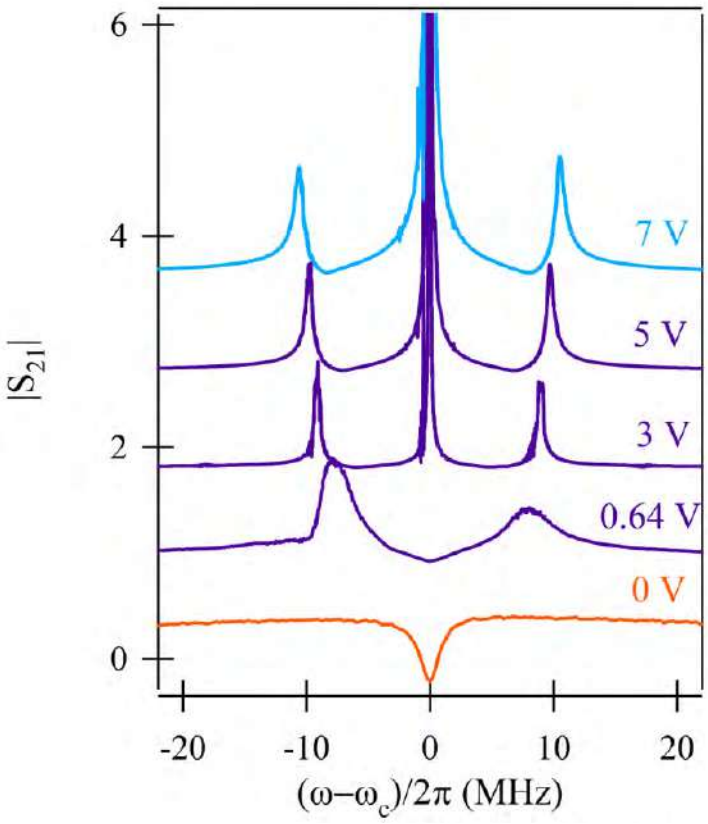

Figure 21: Waterfall plot at $\Delta = 0$ under different bias voltages with fixed YIG sphere. Spectrum is MIT at $V = 0$, Strong coupling at $V = 0.64V$ and magnon quintuplet at $V \geq 2V$. The Rabi frequency Ω_f rise with the increase of applied voltage.

This experiment was performed at $\Delta = 0$ by tuning the H field. The spectra were obtained under different bias voltage from 0 to 7V shown in the waterfall plot in Fig.21 and the Rabi frequency at $\Delta = 0$ is found to be dependent on the voltage. To derive a quantitative description, the Rabi frequency can be simplified to:

$$\Omega_{\pm} = \Omega_f = \Omega_0\sqrt{1 + 2f^2} \tag{81}$$

which means that the two sets of dress states have the same Rabi splitting. Therefore, they produce the same triplet at ω_c and $\omega_c \pm \Omega_f$ as observed in Fig.20(c). The Rabi frequency of this CMP system is dependent only on the coupling strength Ω_0 of MIT and feedback factor f. Rabi frequencies under different voltages are plotted in Fig.22(a), the relation between Ω and V can be described by a empirical linear

formula:

$$\frac{\Omega_f}{\Omega_0} = 1 + k \cdot V \tag{82}$$

Where $\Omega_0 = 15.24$ MHz come from measurement and $k = 5.56 \times 10^{-2}$ is a empirical parameter. Combining Eq.82 and Eq.81 gives the voltage dependent feedback factor:

$$f = \sqrt{k \cdot V + \frac{k^2 V^2}{2}} \tag{83}$$

Where k is the same empirical parameter in Eq.82 with the same value. The measured data and fitting is shown in Fig.22 which shows to be in excellent agreement with our hypothesis.

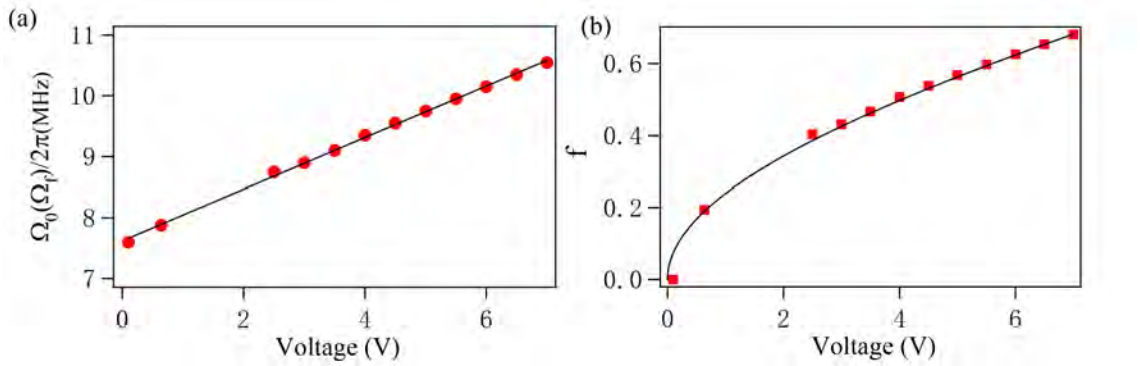

Figure 22: Voltage dependent feedback: (a) Rabi frequencies plotted as a function of bias voltage, there is a approximately a linear relation. (b)The measured(red squares) and calculated(curve) ratio of Rabi frequencies Ω_f/Ω_0 plotted as a function of Gain.

In this experiment, since the position of the YIG sphere is fixed and the microwave magnetic field that is felt by the magnon remains the same under different voltages. By assuming the procession angle of the collective spin or the number of CMP is a constant, tuning the voltage on the feedback loop will increase the number of feedback photons n in Eq.73 which will eventually result in the feedback factor f increasing. Therefore, this voltage controlled feedback brings an additional degree of freedom to the study CMP coupling.

4.6 Distance Dependent Feedback

Another series of experiment where performed to determine the relationship between the distance of the YIG and the feedback factor. During this set of measurements, the distance d of the YIG sphere was changed from 0.2 mm to 2.0 mm by tuning the X-Y-Z stage, the spectrum under V =0 and V =7V was collected to

determine Ω_0 and Ω_f and the waterfall plot is shown in Fig.23. With the distance increasing, $\Omega_0/2\pi$ in MIT dropped from 11 MHz to 3.7 MHz and Ω_f decreased from 15 MHz to 7.7 MHz.

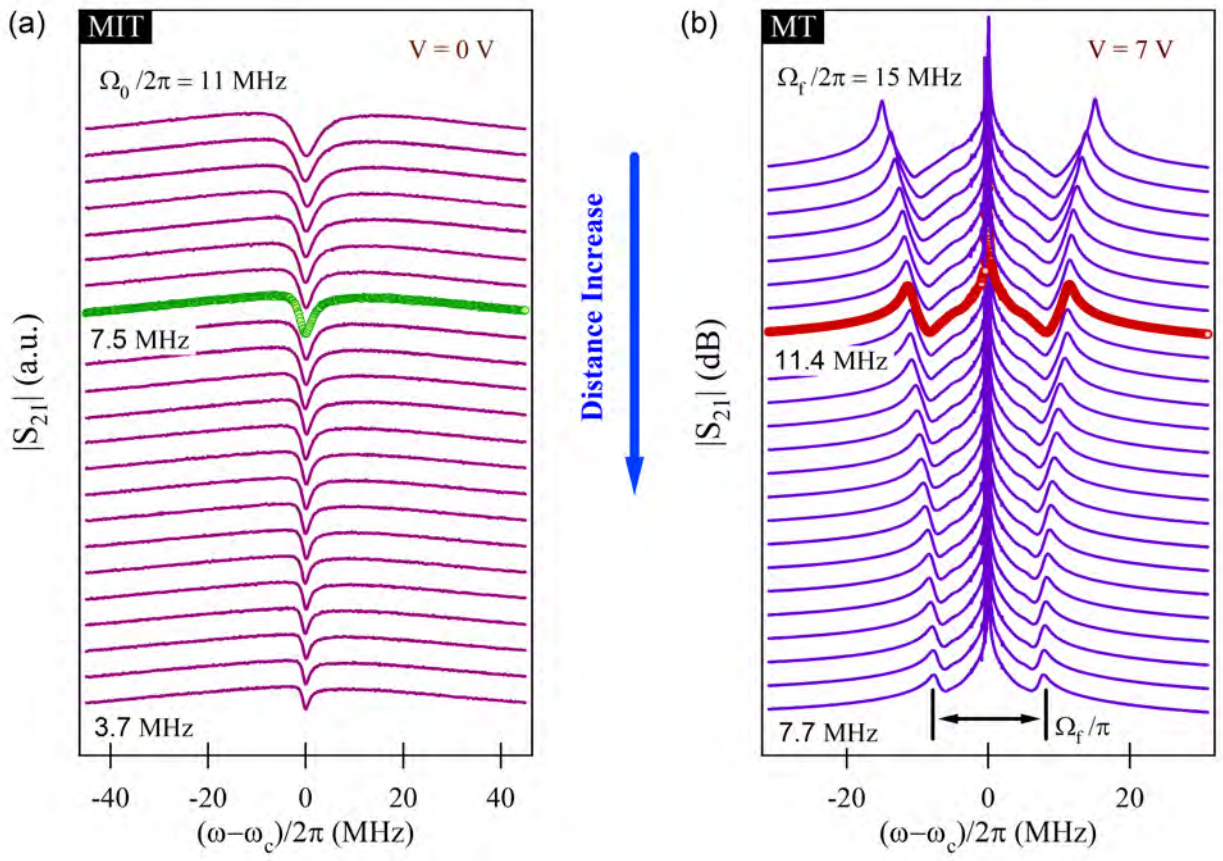

Figure 23: Waterfall plot of MIT in (a) and magnon triplet (MT) in (b), three sets of values for $\Omega_0/2\pi$ and $\Omega_0/2\pi$ are given. Rabi frequency for both MIT and MT have a tendency to decrease as distance d increase.

From these spectra, Ω_0 is acquired by using fitting formula Eq.79 and Ω_f by reading out the peak positions. These results are plotted in Fig.24(a). From Eq.81, the feedback factor is given by:

$$f = \sqrt{\frac{(\Omega_f/\Omega_0)^2 - 1}{2}} \tag{84}$$

Calculated feedback factors f are plotted as a function of distance d, we found that the feedback factor has a linear relation with distance d (Fig.23 (b)):

$$f = 0.35 \cdot d + 0.55 \tag{85}$$

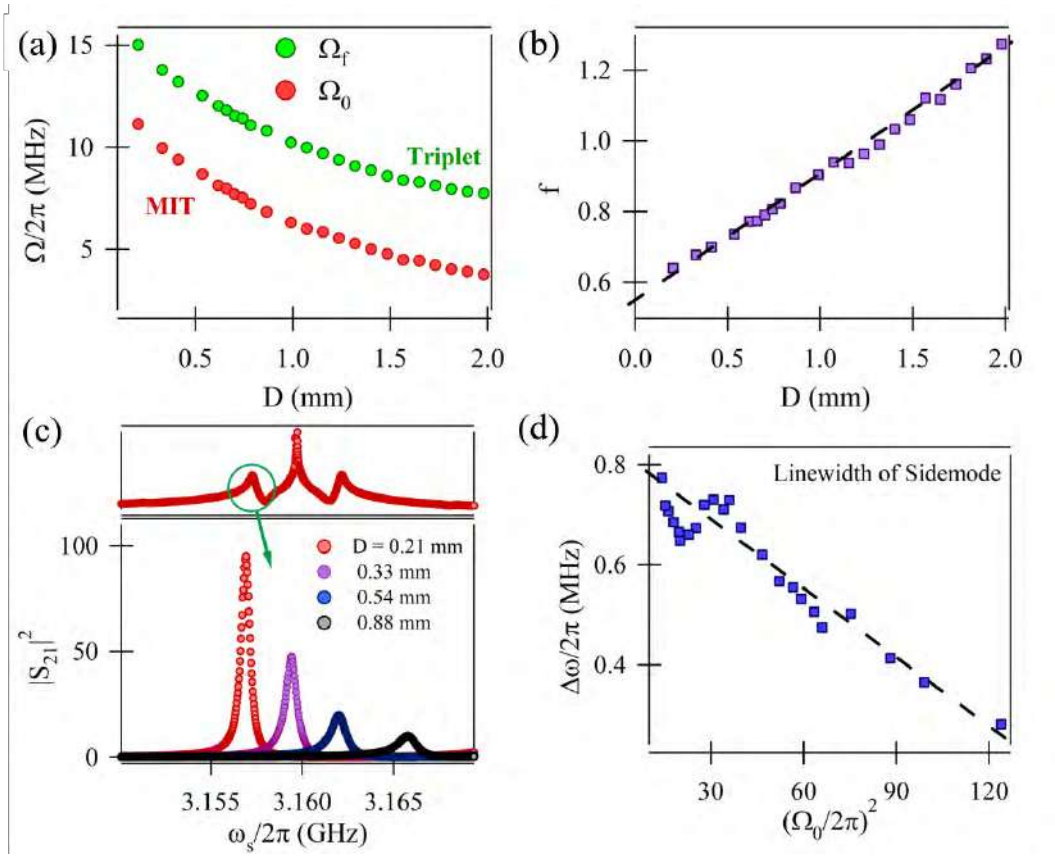

Figure 24: (a) Rabi frequency Ω_0 (red circle) and Ω_f (green circle) extracted from Fig.23, both quantities decreased when d increase. (b) Feedback factors calculated using Eq.84, the linear dependence on distance can be clearly observed, the dashed line is linear fitting of data. (c) Schematic diagram of side mode (top) of magnon triplet and side mode lineshape under different distance d (bottom). The linewidth we get increase with distance d which corresponds to mean lifetime of CMP. (d) The linewidth of the side mode plotted as a function of the square of the coupling strength $(\Omega_0/2\pi)^2$, data points (markers) were fitted by a linear relation.

Furthermore, we analysed the linewidth $\Delta\omega$ of the side mode of magnon triplet which correspond to the mean lifetime $\tau = 1/(2\pi\Delta\omega)$ of CMP. The linewidth was plotted as a function of the coupling strength $(\Omega_0/2\pi)^2$ which is linearly fitted as:

$$\frac{\Delta\omega}{2\pi} = -4.21\text{THz}^{-1} \cdot (\frac{\Omega_0}{2\pi})^2 + 0.797\text{MHz} \tag{86}$$

Therefore, we have determined the relationship between the feedback factor and the distance. Furthermore, the relation of the linewidth $\Delta\omega$ of the side mode and the square of coupling strength Ω_0 at $\Delta = 0$ is approximately a linear relation has been found. Based on this assumption, the mean lifetime of the CMP as a function of

$(\Omega_0/2\pi)^2$ can be guessed to be:

$$\tau = \frac{1}{a(\Omega_0/2\pi)^2 + b} \tag{87}$$

Where a and b are fitting parameters. Mean lifetime τ is expected to decrease with square of coupling strength Ω_0. In this experiment, the feedback factor f has been proved to be dependent on the distance d. The linewidth $\Delta\omega$ and the mean lifetime τ with respected to the coupling strength Ω_0 has been discussed. This may provide potential application on further development of cavity magnon polariton and spin dynamics.

5 Conclusion

A novel design of active cavity with the A-P design provides us with a powerful tool for the study of cavity spintronics and spin dynamics. In this research, we have studied ferromagnetic material interacting with a feedback loop cavity in the newly developing field of cavity spintronics. Coupling of cavity photons and magnons can be explained by both classical and quantum theory. Strong interaction between these two modes can generate CMP which have an anti-crossing behavior and the quintuplet that has been recently observed. It is clear that classical and quantum model can describe the anti-crossing with similar results, while the quintuplet can only be explained by quantum theory currently. Based on a theoretical explanation of magnon quintuplet, we defined the feedback factor f using Rabi frequencies of the A-P-M system.

We have demonstrated a highly tuneable coupling system on a planar structure at room temperature. Usually the coupling strength characterized by Rabi frequency is independent of the photon numbers in cavity. However, in this work, by tuning the bias voltage which results in an increase in the feedback photons, the coupling strength as well as the coupling regime are changed. The relation of f as a function of voltage V have been derived and agreed well with experiment data. Furthermore, data presented has clearly demonstrated the coupling strength Ω_f is also dependent on position of YIG sphere. This approach is tuning the distance d between A-P cavity and magnon which result drop of the number of polaritons to change the f. We found f has a linear relation with d. In addition to this, we found the linewidth of CMP mode has an approximately linear relation with the square of the coupling strength Ω_0^2.

Based on this work, the understanding of the coupling between magnons and cavity photons with feedback loop has been improved, and this experiment setup provides the potential to integrate to on-chip device that use voltage and distance control the information procession properties in spintronics.

6 Future Work

For the theory of cavity magnon quintuplet we introduced in section 2.3.3, it can only explain the dispersion relation of this coupling regime but can do nothing for the damping of the five modes, especially the central mode of the active cavity. However, through the fitting data plotted in Fig.20(d), the properties of the linewidth revolution is still able to be seen. The next step is developing this current quantum theory by adding damping terms which could take a lot of efforts.

In this research, we have explored MIT, strong coupling and cavity magnon quintuplet in three different coupling regimes. However there is still another coupling regime called Purcell effect where the damping of the ferromagnetic material dominate ($\kappa_a < g < \kappa_m$) which has yet to be determined. Purcell effect will enhance the decay of the photon cavity due to the coupling between a high damping material. Magnetic nano-particles, Permalloy sphere are good candidates for this further research instead of YIG sphere. Interesting phenomena that differs from passive cavity can be expected due to the presence of feedback loop and it can also improve our understanding of this A-P-M device.

Acknowledgement

First, I want to thank Dr.Can-Ming Hu and Dr.Yongsheng Gui who have provided their valuable advises and guidance over the past eight months, and Jinwei Rao that provided countless detail help and a brother-like support on this project, Ying Yang for doing iFFT calculation and Kelsey Wiebe for correcting grammar errors. Thank you to all other group members of Dynamic Spintronics Group who have together create a healthy and friendly environment for doing research. Finally, I want to express my appreciation to my family (father, mother and girlfriend), without their support both mentally and physically, there is no chance for me to finish this work.

References

[1] D. Sanvitto and S. Kéna-Cohen, "The road towards polaritonic devices," *Nature materials*, vol. 15, no. 10, p. 1061, 2016.

[2] K. Tolpygo, "Physical properties of a rock salt lattice made up of deformable ions," *Ukr. J. Phys*, vol. 53, pp. 93–102, 2008.

[3] K. Huang, "Lattice vibrations and optical waves in ionic crystals," *Nature*, vol. 167, no. 4254, p. 779, 1951.

[4] D. Mills and E. Burstein, "Polaritons: the electromagnetic modes of media," *Reports on Progress in Physics*, vol. 37, no. 7, p. 817, 1974.

[5] E. L. Albuquerque and M. G. Cottam, *Polaritons in periodic and quasiperiodic structures*. Elsevier, 2004.

[6] L. Landau, "On the theory of the dispersion of magnetic permeability in ferromagnetic bodies," *Phys. Z. Sowjet.*, vol. 8, pp. 153–169, 1935.

[7] J. Griffiths, "Anomalous high-frequency resistance of ferromagnetic metals," *Nature*, vol. 158, no. 4019, p. 670, 1946.

[8] E. Zavoisky, "Spin magnetic resonance in the decimetre-wave region," *J. Phys. USSR*, vol. 10, pp. 197–198, 1946.

[9] ——, "Paramagnetic absorption in some salts in perpendicular magnetic fields," *Zhurnal Eksperimentalnoi I Teoreticheskoi Fiziki*, vol. 16, no. 7, pp. 603–606, 1946.

[10] C. Kittel, "On the theory of ferromagnetic resonance absorption," *Physical Review*, vol. 73, no. 2, p. 155, 1948.

[11] A. Chumak, V. Vasyuchka, A. Serga, and B. Hillebrands, "Magnon spintronics," *Nature Physics*, vol. 11, no. 6, p. 453, 2015.

[12] F. Bloch, "Zur theorie des ferromagnetismus," *Zeitschrift für Physik*, vol. 61, no. 3-4, pp. 206–219, 1930.

[13] M. á. Kostylev, A. Serga, T. Schneider, B. Leven, and B. Hillebrands, "Spin-wave logical gates," *Applied Physics Letters*, vol. 87, no. 15, p. 153501, 2005.

[14] S. Ramo, J. R. Whinnery, and T. Van Duzer, *Fields and waves in communication electronics*. John Wiley & Sons, 2008.

[15] J. Rao, S. Kaur, X. Fan, D. Xue, B. Yao, Y. Gui, and C.-M. Hu, "Characterization of the non-resonant radiation damping in coupled cavity photon magnon system," *Applied Physics Letters*, vol. 110, no. 26, p. 262404, 2017.

[16] S. Kaur, "Study of on-chip cavity magnon polariton devices," *Master Thesis, University of Manitoba*, 2017.

[17] M. H. Zarifi, T. Thundat, and M. Daneshmand, "High resolution microwave microstrip resonator for sensing applications," *Sensors and Actuators A: Physical*, vol. 233, pp. 224–230, 2015.

[18] M. H. Zarifi and M. Daneshmand, "Non-contact liquid sensing using high resolution microwave microstrip resonator," in *Microwave Symposium (IMS), 2015 IEEE MTT-S International*. IEEE, 2015, pp. 1–4.

[19] M. H. Zarifi, M. Fayaz, J. Goldthorp, M. Abdolrazzaghi, Z. Hashisho, and M. Daneshmand, "Microbead-assisted high resolution microwave planar ring resonator for organic-vapor sensing," *Applied Physics Letters*, vol. 106, no. 6, p. 062903, 2015.

[20] B. Yao, Y. Gui, J. Rao, S. Kaur, X. Chen, W. Lu, Y. Xiao, H. Guo, K.-P. Marzlin, and C.-M. Hu, "Cooperative polariton dynamics in feedback-coupled cavities," *Nature Communications*, vol. 8, no. 1, p. 1437, 2017.

[21] C.-M. HU, "Dawn of cavity spintronics," *PHYSICS IN CANADA*, vol. 72, no. 2, 2016.

[22] B. Yao, Y. Gui, M. Worden, T. Hegmann, M. Xing, X. Chen, W. Lu, Y. Wroczynskyj, J. van Lierop, and C.-M. Hu, "Quantifying the complex permittivity and permeability of magnetic nanoparticles," *Applied Physics Letters*, vol. 106, no. 14, p. 142406, 2015.

[23] B. Yao, Y. Gui, Y. Xiao, H. Guo, X. Chen, W. Lu, C. Chien, and C.-M. Hu, "Theory and experiment on cavity magnon-polariton in the one-dimensional configuration," *Physical Review B*, vol. 92, no. 18, p. 184407, 2015.

[24] S. Kaur, B. Yao, J. Rao, Y. Gui, and C.-M. Hu, "Voltage control of cavity magnon polariton," *Applied Physics Letters*, vol. 109, no. 3, p. 032404, 2016.

[25] S. Kaur, B. Yao, Y.-S. Gui, and C.-M. Hu, "On-chip artificial magnon-polariton device for voltage control of electromagnetically induced transparency," *Journal of Physics D: Applied Physics*, vol. 49, no. 47, p. 475103, 2016.

[26] X. Zhang, C.-L. Zou, L. Jiang, and H. X. Tang, "Strongly coupled magnons and cavity microwave photons," *Physical review letters*, vol. 113, no. 15, p. 156401, 2014.

[27] M. Harder, L. Bai, C. Match, J. Sirker, and C. Hu, "Study of the cavity-magnon-polariton transmission line shape," *Science China Physics, Mechanics & Astronomy*, vol. 59, no. 11, p. 117511, 2016.

[28] Ö. O. Soykal and M. Flatté, "Strong field interactions between a nanomagnet and a photonic cavity," *Physical review letters*, vol. 104, no. 7, p. 077202, 2010.

[29] H. Huebl, C. W. Zollitsch, J. Lotze, F. Hocke, M. Greifenstein, A. Marx, R. Gross, and S. T. Goennenwein, "High cooperativity in coupled microwave resonator ferrimagnetic insulator hybrids," *Physical Review Letters*, vol. 111, no. 12, p. 127003, 2013.

[30] M. Goryachev, W. G. Farr, D. L. Creedon, Y. Fan, M. Kostylev, and M. E. Tobar, "High-cooperativity cavity qed with magnons at microwave frequencies," *Physical Review Applied*, vol. 2, no. 5, p. 054002, 2014.

[31] X. Zhang, C.-L. Zou, N. Zhu, F. Marquardt, L. Jiang, and H. X. Tang, "Magnon dark modes and gradient memory," *Nature communications*, vol. 6, p. 8914, 2015.

[32] Y. Tabuchi, S. Ishino, A. Noguchi, T. Ishikawa, R. Yamazaki, K. Usami, and Y. Nakamura, "Coherent coupling between a ferromagnetic magnon and a superconducting qubit," *Science*, vol. 349, no. 6246, pp. 405–408, 2015.

[33] D. M. Pozar, *Microwave engineering*. John Wiley & Sons, 2009.

[34] C. Liu, Z. Dutton, C. H. Behroozi, and L. V. Hau, "Observation of coherent optical information storage in an atomic medium using halted light pulses," *Nature*, vol. 409, no. 6819, p. 490, 2001.

[35] J. P. Marangos, "Electromagnetically induced transparency," *Journal of Modern Optics*, vol. 45, no. 3, pp. 471–503, 1998.